Pergamon

Geochimica et Cosmochimica Acta, Vol. 68, No. 21, pp. 4405–4427, 2004

0016-7037/04 $30.00 + .00

doi:10.1016/j.gca.2004.04.016

Mineralogical, geochemical and isotopic characteristics of hydrothermal alteration processes in the active, submarine, felsic-hosted PACMANUS field, Manus Basin, Papua New Guinea

K. S. Lackschewitz,[1,3,*] C. W. Devey,[1,3] P. Stoffers,[2] R. Botz,[2] A. Eisenhauer,[3] M. Kummetz,[4] M. Schmidt,[2] and A. Singer[5]

[1]Fachbereich Geowissenschaften, Universität Bremen, 24334 Bremen, Germany
[2]Institut für Geowissenschaften, Universität Kiel, 24118 Kiel, Germany
[3]FM-GEOMAR, Leibniz-Institute für Meereswissenschaften 24124 Kiel, Germany
[4]Universum, Science Center, 24334 Bremen, Germany
[5]Seagram Center for Soil and Water Sciences, Hebrew University of Jerusalem, 76100 Rehovot, Israel

(*Received May* 13, 2003; *accepted in revised form April* 15, 2004)

Abstract—During ODP Leg 193, 4 sites were drilled in the active PACMANUS hydrothermal field on the crest of the felsic Pual Ridge to examine the vertical and lateral variations in mineralization and alteration patterns. We present new data on clay mineral assemblages, clay and whole rock chemistry and clay mineral strontium and oxygen isotopic compositions of altered rocks from a site of diffuse low-temperature venting (Snowcap, Site 1188) and a site of high-temperature venting (Roman Ruins, Site 1189) in order to investigate the water-rock reactions and associated elemental exchanges.

The volcanic succession at Snowcap has been hydrothermally altered, producing five alteration zones: (1) chlorite ± illite-cristobalite-plagioclase alteration apparently overprinted locally by pyrophyllite bleaching at temperatures of 260–310°C; (2) chlorite ± mixed-layer clay alteration at temperatures of 230°C; (3) chlorite and illite alteration; (4) illite and chlorite ± illite mixed-layer alteration at temperatures of 250–260°C; and (5) illite ± chlorite alteration at 290–300°C. Felsic rocks recovered from two holes (1189A and 1189B) at Roman Ruins, although very close together, show differing alteration features. Hole 1189A is characterized by a uniform chlorite-illite alteration formed at ~250°C, overprinted by quartz veining at 350°C. In contrast, four alteration zones occur in Hole 1189B: (1) illite ± chlorite alteration formed at ~300°C; (2) chlorite ± illite alteration at 235°C; (3) chlorite ± illite and mixed layer clay alteration; and (4) chlorite ± illite alteration at 220°C.

Mass balance calculations indicate that the chloritization, illitization and bleaching (silica-pyrophyllite assemblages) alteration stages are accompanied by different chemical changes relative to a calculated pristine precursor lava. The element Cr appears to have a general enrichment in the altered samples from PACMANUS. The clay concentrate data show that Cr and Cu are predominantly present in the pyrophyllites. Illite shows a significant enrichment for Cs and Cu relative to the bulk altered samples.

Considerations of mineral stability allow us to place some constraints on fluid chemistry. Hydrothermal fluid pH for the chloritization and illitization was neutral to slightly acidic and relatively acidic for the pyrophyllite alteration. In general the fluids, especially from Roman Ruins and at intermediate depths below Snowcap, show only a small proportion of seawater mixing (<10%). Fluids in shallow and deep parts of the Snowcap holes, in contrast, show stronger seawater influence.

1. INTRODUCTION

The PACMANUS hydrothermal field (named after the Papua New Guinea-Australia-Canada-Manus cruise with RV *Franklin* in 1991 which discovered the field), drilled during the Ocean Drilling Program (ODP) Leg 193, is the first active felsic-hosted convergent margin hydrothermal system to be studied by scientific drilling.

Several studies have shown that the host rock composition is important in determining the character and composition of wall rock alteration and sulfide mineralization (e.g., Zierenberg and Shanks, 1994; Hannington et al., 1995; Barrie and Hannington, 1999; Alt and Bach, 2003). Studies of hydrothermal precipitates have demonstrated that felsic-hosted sulfide deposits are particularly rich in gold relative to those at typical basalt-hosted hydrothermal fields on midocean ridges (e.g., Herzig et al., 1993; Herzig and Hannington, 2000; Moss et al., 2001).

Most of the formerly igneous/volcanic rocks recovered during Leg 193 are characterized by extensive hydrothermal alteration displaying an extreme diversity of mineral assemblages including silicates, sulfides, sulfates and oxides (Binns et al., 2002). These assemblages reflect a complex variety of alteration conditions. Phyllosilicates, in addition to cristobalite and quartz, are the dominant hydrothermal alteration minerals and are therefore important for understanding the alteration conditions, especially with respect to the chemical and isotopic exchange between felsic rocks and hydrothermal fluids. A detailed characterization of clay minerals is fundamental to understanding the changing physicochemical parameters of the fluids in the felsic-hosted hydrothermal system of PACMANUS. In general, studies of hydrothermal clays have been focussed on basalt-hosted hydrothermal fields located at mid-ocean ridges. Several studies on hydrothermal clay minerals

* Author to whom correspondence should be addressed (klackschewitz@ifm.geomar.de).

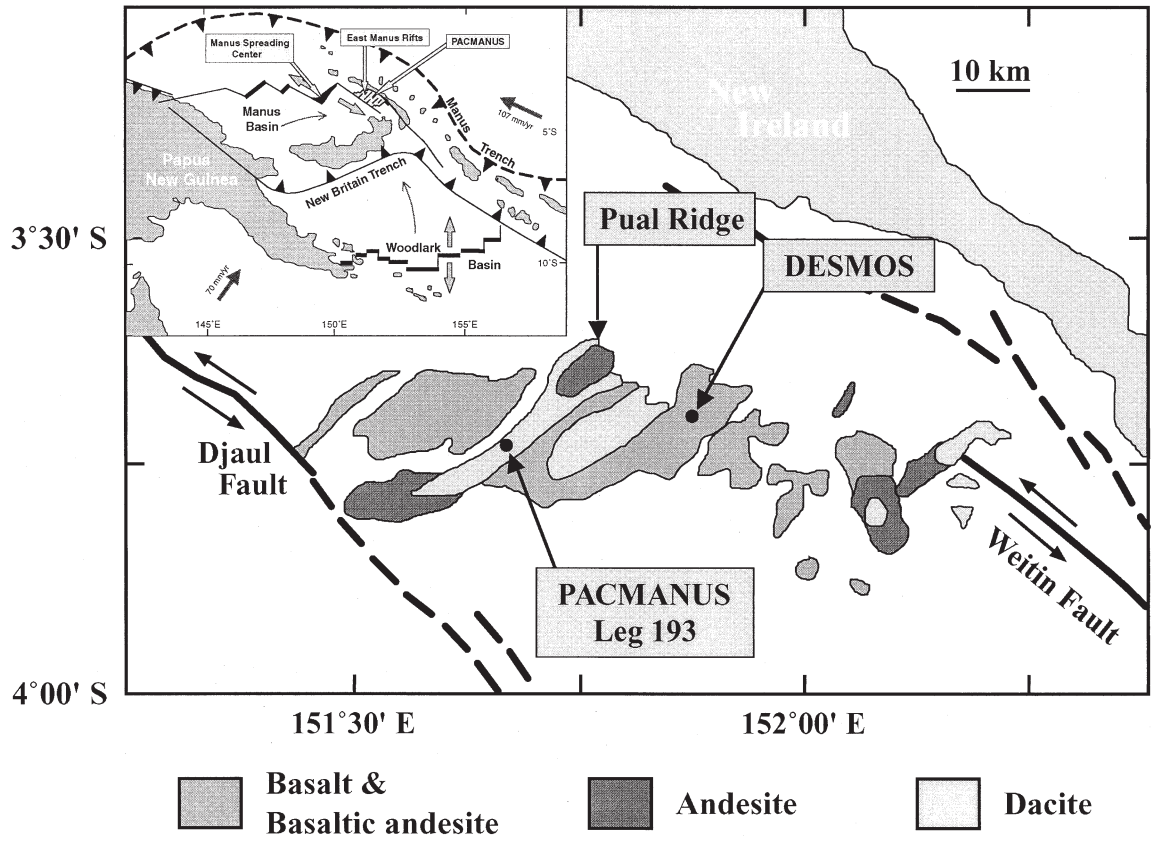

Fig. 1. Seafloor geology of the eastern Manus Basin. ENE-trending neovolcanic edifices, extending between the active ends of the Djaul and Weitin transform faults, have yielded lavas ranging from picritic basalt to rhyodacite in composition (modified after Binns et al. 2002). Inset shows the regional tectonic setting of the PACMANUS hydrothermal site in the eastern Manus Basin. PACMANUS lies in the eastern Manus Rift zone, a pull-apart structure between two major transform faults (modified after Binns et al., 2002).

from midocean ridge systems have documented diverse alteration assemblages that reflect histories of changing chemical and physical conditions (e.g., Honnorez et al., 1983; Singer and Stoffers, 1987; Buatier et al., 1989, 1995; Lackschewitz et al., 2000a,b; Porter et al., 2000).

Previous studies of the clay mineral alteration from drill holes in felsic volcanic arc and back-arc basement (e.g., Schöps and Herzig, 1994; Alt et al., 1998; Vitali et al., 1999) have documented locally intense alteration with the formation of illite, chlorite, kaolinite, pyrophyllite and diverse mixed-layers. However, only little is known about the chemical and isotopic changes during the alteration and mineralization of felsic-hosted hydrothermal systems.

This paper presents mineralogical, chemical and isotopic data for hydrothermal phyllosilicates from Ocean Drilling Program (ODP) Sites 1188 and 1189 at the hydrothermally active PACMANUS site in the Manus Basin, drilled during ODP Leg 193. Analysis of clay separates representing a variety of alteration styles demonstrates that significant and characteristic changes in the bulk rock chemical composition are associated with the various stages of the high-temperature alteration. An estimation of the chemical exchange for the different alteration styles allows us to document the elemental gains and losses during alteration and to document the physical and chemical variables in the fluids that control the alteration mineral paragenesis.

2. GEOLOGIC SETTING

2.1. Regional Setting

The Manus Basin in the eastern Bismarck Sea is a fast-opening (ca. 10 cm/yr) backarc basin that is bound by the inactive Manus Trench in the north and the active New Britain Trench in the south (Fig. 1).

The eastern Manus basin is a pull-apart zone which is bounded by two major transform faults, the Weitin Fault to the east and the Djault Fault to the west (Fig. 1). Between these transforms a series of en echelon volcanic ridges were formed by fissure eruptions of calcalkaline volcanics. Several of these neovolcanic zones are characterized by widespread hydrothermal activity.

The PACMANUS hydrothermal field is one of three major hydrothermally active areas in the eastern Manus Basin lying on the crest of the northeast-trending Pual Ridge (Fig. 1). The ridge is composed predominantly of dacite and andesite (Binns and Scott, 1993; Paulick et al., 2004). Hydrothermal activity at PACMANUS is concentrated in several discrete fields, including active chimney fields, iron-oxide mounds, and areas of

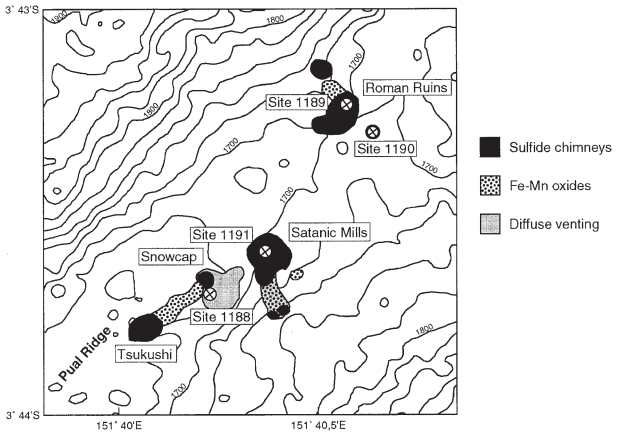

Fig. 2. Distribution of hydrothermal deposits within the PACMANUS field along the crest of Pual Ridge and location of ODP Leg 193 drill hole sites. The map is based on bottom-tow photography and submersible dive observations from several PACMANUS cruises (modified after Binns et al., 2002).

diffuse venting, over a 3-km section of the Pual Ridge crest (Fig. 2). Cores from the following two fields were used in this study:

Roman Ruins (1693–1710 mbsl, 150 m across) is characterized by many columnar chimneys as high as 20 m expelling high temperature black-smoker fluids (T = 268°C). End-member fluids are acidic (pH = 2.7), have high K/Ca ratios, and are high in Mn, Fe, and Pb relative to midocean ridge fluids (Auzende et al., 1996; Shitashima et al., 1997; Douville 1999).

Snowcap (1654–1670 mbsl) is a site of low-temperature (6°C) diffuse venting. It is a 10 to 15 m high hill, 100 × 200 m in size, of altered dacite-rhyodacite and hyaloclastite. Alteration minerals such as cristobalite, alunite, diaspore and illite-montmorillonite predominate reflecting interaction at low-temperature between dacites and a highly acid, relatively oxidized hydrothermal fluid, i.e., advanced argillic alteration (Binns et al., 2002).

2.2. Hydrothermal Alteration

Active PACMANUS hydrothermal sites were penetrated on ODP Leg 193 in holes 1188A, 1188F (both Snowcap), 1189A, 1189B (both Roman Ruins), and 1191A (Satanic Mills) (Binns et al., 2002; Fig. 2). The Satanic Mills site 1191 was penetrated to only 20.1 mbsf and had very poor core recovery with negligible alteration so will not be examined further.

With the exception of fresh glassy rhyodacite and dacite near the seafloor, hydrothermal alteration is ubiquitous in the subsurface at Snowcap and Roman Ruins (Binns et al., 2002). The hydrothermal alteration is complex and multi-stage, and includes pervasive replacement of igneous material, and alteration halos along anhydrite ± pyrite ± quartz veins. Mineral assemblages arising from hydrothermal alteration vary with depth, and are complicated by overprinting relationships. At both sites, rocks are highly to completely altered to cristobalite and/or quartz, clay minerals, anhydrite and disseminated pyrite. A lower sequence below 120 mbsf in Hole 1189B comprises hydrothermal alteration features which are distinctly different from those encountered at Snowcap. K-feldspar is abundant and magnetite is rare. The K-feldspar appears to be associated with quartz-chlorite alteration, which alternates with less strongly altered cristobalite-bearing rocks in the lower portion of Hole 1189B. For a detailed description of the petrography of the samples the reader is referred to the ODP Initial Results volume (Binns et al., 2002).

3. METHODS

The water-saturated samples were freeze-dried for disintegration. After weighing, the freeze-dried sample was divided into a fine (<63 μm) and a coarse fraction (>63 μm) by wet sieving. Grain size separation into a silt (2–63 μm) and a clay fraction (<2 μm) was performed by settling of particles in standing cylinders according to Stokes' law (Moore and Reynolds, 1989). In addition, some clay fractions were separated into a <1 μm- and a 1–2 μm-fraction using a centrifuge. In the latter case we were able to produce clay mineral separates for three samples for oxygen and strontium isotope analyses.

Clay mineralogy was determined by X-ray diffractometry using a Philips X-ray diffractometer PW 1710 with monochromatic Cu-Kα radiation. Oriented samples were produced by vacuum filtration through a 0.2 μm filter. Measurements were carried out on air-dried, glycol-saturated and KCl-saturated samples. Randomly oriented powder preparations were scanned from 60 to 75° 2 theta to identify di- or trioctahedral clay minerals from their 060 reflections. Relative abundances of the minerals are estimated qualitatively using the following categories: trace (<2%), minor (2–5%), common (5–50%), abundant (50–90%) and very abundant (>90%).

Based on structural and chemical data Brindley and Brown (1980) calculated XRD profiles for illite-dioctahedral chlorite and illite-(glycol) dioctahedral smectite with different proportions of smectite using a computer program that treats three-component interstratification. They documented that significant changes in the amount of one component affect the position of the peaks. Thus, careful measurement of the spacing of these peaks gives compositional information for mixed layer clays from the *d*-values of Brindley and Brown (1980).

Simultaneous thermogravimetric analysis (TGA) and differential thermal analysis (DTA) were carried out on 10 mg of powdered samples with a TA Instruments (USA) model SDT 2960. TGA/DTA runs were recorded at a scan rate of 10°C/min up to 1100°C. The sample compartment was flushed at all times with dried, ultra-high-purity argon. Infrared spectroscopy (IRS) was carried out on a Nicolette FTIR apparatus. Infrared spectra were registered in the 4000–400 cm^{-1} range using nearly monomineralic samples prepared in the form of KBr disks. For major and trace element analysis, bulk rock samples were oven-dried at 40°C and then pulverized. The major element composition of bulk rock samples and clay concentrates was determined using Philips (PW 1400 and PW 1480) X-ray fluorescence (XRF) spectrometers and a Camebax SX 50 electron microprobe, respectively. For XRF analysis, the samples were dried at 900°C and melted using lithium tetraborate ($Li_2B_4O_7$) in a mixture consisting of 600 mg rock powder and 3600 mg lithium tetraborate. The XRF determinations were calibrated against 44 international rock standards. Electron microprobe analyses were performed on pressed-powder pellets. To effectively average compositional heterogeneities, four to eight points were analyzed on each clay concentrate by a defocussed beam. Trace elements were analyzed using a Finnigan MAT Element 2 double-focussing, single collector ICP-MS. Total dissolution of bulk rock samples and clay concentrates was performed by a microwave HF-HNO_3-aqua regia attack (Garbe-Schönberg, 1993). The accuracy of the analytical results was controlled by measuring the international standard reference material "BHVO-2."

For oxygen isotope analysis, only samples with monomineralic clays (as determined by XRD) were analyzed. before isotope analysis, free Fe- and Mn-oxides were removed by the method of Mehra and Jackson (1960). Oxygen was extracted from silicates using the ClF_3 method (Clayton and Mayeda, 1963; Borthwick and Harmon, 1982). The samples were transferred to nickel reaction vessels and heated for 2 h at 150°C. All samples were then reacted with ClF_3 at 600°C for 12 h. Oxygen was quantitatively converted to CO_2 which then was analyzed

isotopically in a Finnigan MAT 251 stable isotope mass spectrometer. Oxygen isotope ratios are expressed in the conventional δ-notation as deviation in per mil from SMOW (Standard Mean Ocean Water). The oxygen isotope value of the NBS-28 standard (Matsuhisa, 1974) was determined to be $\delta^{18}O = 9.2 \pm 0.2‰$ (accepted value 9.6 ± 0.15‰)

Sr-isotope composition was measured with the Re-double filament technique on a Finnigan MAT 262 RPQ^+ in static mode. Usually 100 to 200 $^{87}Sr/^{86}Sr$ ratios were collected for each measurement, which resulted in a internal precision of better than 10 ppm (2 SE) of the $^{87}Sr/^{86}Sr$ value for most of the samples. The whole procedure Sr blank is less than 500 pg. However, sample sizes are sufficiently large (approx. 1 μg of Sr) that blank corrections are negligible. A mean $^{87}Sr/^{86}Sr$ value of 0.710236 ± 34 (2 standard deviations) for the NIST 987 standard solution was calculated from 12 analyses (accepted value 0.71025), covering the whole measurement period for the data set. The ± 34 represents the minimum uncertainty assigned to any individual sample measurement.

4. RESULTS

4.1. X-ray Diffraction Data

The clay mineral assemblages obtained by XRD are reported in Tables 1, 2 and 3.

4.1.1. Snowcap

The clay mineralogy of samples from holes 1188A and 1188F is dominated by illite and chlorite (Table 1). Chlorite was identified by the (001) spacing at 14.2 Å which remains unaffected by glycol saturation or heating at 550°C. TGA/DTA and IRS of a nearly pure chlorite in the clay fraction of sample 1188A-20R-1, 68–72 cm indicate a trioctrahedral 2:1 layer. Reflections at ~10 Å and 5.0 Å characterize illite. In addition, a reflection at 14.2–14.5 Å, which expands to 17.0–17.2 Å after glycolation, indicates the presence of smectites in some of these samples. Reflections between 12 and 13 Å in KCl-saturated samples are also typical of smectite (e.g., Sample 1188A-8R-1, 108–112 cm). A (060) reflection at 1.495 Å indicates dioctahedral smectite.

The appearance of illite-smectite-chlorite (I-S-C) mixed layers characterizes the clay mineralogy of the uppermost sample 1188A-7R-1, 88–92 cm at 49.08 mbsf. Strong reflections at 14.2 Å, 7.1 Å, 4.74 Å and 3.54 Å changed after glycol treatment to 15.9 Å, 8.3 Å and 7.53 Å, 5.53 Å, and to a broad reflection in the region 3.54–3.40 Å, respectively, confirming the presence of an I-S-C phase (Brindley and Brown, 1980). A small reflection at 9.6 Å indicates the presence of illite interlayers. The XRD patterns produced by air-dried, glycolated samples of pervasively bleached, acid sulfate-altered rocks show basal reflections at 9.4 to 9.5 Å, 4.65 to 4.7 Å and 3.09 to 3.11 Å (Fig. 3A) which can be attributed to either pyrophyllite or talc. TGA/DTA, IRS and chemical analyses confirm the presence of pyrophyllite. Pyrophyllite occurs as a nearly pure mineral in four clay concentrates between 49 and 120 mbsf in Hole 1188A (see Table 1), with trace amounts of pyrite or anhydrite or quartz. Cristobalite and plagioclase are additional common phases in the clay fractions of samples between 50 and 170 mbsf.

At 120 to 190 mbsf, the mineralogical sequence reflects a distinct change to illite-smectite (I-S) and chlorite-vermiculite-smectite (C-V-S) mixed layer-dominated clay fractions. The I-S is characterized by a diffraction peak at 12.2 Å which becomes 14.2 Å after glycolation (Fig. 3B). Reflections in the region 5.0–5.3 Å confirm the presence of an I-S phase (Moore and Reynolds, 1989). A superlattice peak at 24 Å that expands to 27 Å with glycol was found in sample 1188A-17R-1, 38–41 cm, implying the presence of regular 1:1 interstratification in mixed layering.

Figure 3C is an example of the three-component interstratification chlorite-vermiculite-smectite. The XRD diagram is characterized by several strong basal reflections and a superlattice peak at 28.2 Å. The peak positions of this phase change little after glycolation indicating only small amounts of interlayered smectite. The XRD patterns for the KCl-saturated C-V-S samples, where the reflections collapse from between 29–28 Å, 14.1–14.4 Å and 9 Å to between 25–26 Å, 12.7–13.3 Å and 8.6 Å, respectively, denote a three-component system consisting of chlorite, vermiculite and smectite (Brindley and Brown, 1980; Reynolds, 1988).

The section between 220 and 310 mbsf at Site 1188 is characterized by a clay-mineral assemblage of interlayered illite-chlorite (I-C), or of illite-smectite mixed layer and illite with or without chlorite. I-C contains 40–90% illite whereas I-S comprises 60–70% illite. Interlayered chlorite-vermiculite (C-V) is also present (Fig. 3D). There are traces of quartz in some concentrates. The clay minerals below 310 mbsf are illite and chlorite without expandable layers. Many of the concentrates also contain minor to moderate amounts quartz and plagioclase.

4.1.2. Roman Ruins

The clay mineralogy of the samples from hole 1189A is dominated by chlorite and illite (Table 2). The deepest sample 1189A-13R-1, 23–33 cm at 116.3 mbsf has the highest chlorite content (>90%) of the hole. An IR spectrum shows strong absorption bands which are distinctive for a fully trioctahedral chlorite. Nearly all concentrates contain minor to trace amounts of plagioclase. Quartz is only present in three concentrates below 90 mbsf whereas two concentrates between 10 and 20 mbsf contain relatively high contents of cristobalite.

The clay fractions from 40 to ~50 mbsf of Hole 1189B include illite as a major component together with chlorite (Table 3). Traces of pyrite are restricted to the two uppermost samples. The section between approximately 80 to 120 mbsf is characterized by abundant chlorite together with minor illite, except for a sample at 98.50 mbsf with abundant illite. In addition, a few concentrates contain quartz, plagioclase or potassium feldspar. At the lower sequence of hole 1189B the interval between 127 and 140 mbsf is characterized by the occurrence of illite-vermiculite (I-V) and C-V mixed layers. Reflections in the region 10.5–12.0 Å and 3.3–3.4 Å confirm the presence of an I-V phase with ≥70% illite (Moore and Reynolds, 1989), whereas the superlattice reflection at 29.7 Å and the peak at 14.4 Å indicate a moderate amount of C-V with 60% chlorite in sample 1189B-12R-1, 109–112 cm (Brindley and Brown, 1980). In most of these concentrates cristobalite and/or plagioclase occur as the dominant phase. In most of the samples below 147 mbsf, chlorite again becomes abundant.

4.2. Chemical Composition of Secondary Clay Minerals

Major element compositions of selected clay concentrates are given in Table 4. In the three representative analyses of pyrophyl-

Table 1. Mineralogical assemblages of the clay fraction (<2 μm) of altered falsic rocks from Holes 1188A and 1188F (as determined by X-ray diffraction analyses).[a]

Sample	Depth (mbsf)	Chl	Sm	Ill	Pyroph	Talc	Chl-Sm	Chl-V	Ill-Sm (% Ill)	Ill-Chl (% Ill)	Ill-Sm-Chl	Qz	Cris	Plag	Py	Mag	An
193-1188A-7R-1, 88–92 cm	49.08										xxx			xx			
193-1188A-7R-1, 118–122 cm	49.38	xxx		xx										o	o		
193-1188A-7R-1, 144–148 cm	49.64				xxxx										o		
193-1188A-8R-1, 105–112 cm	58.98	xxx	xxxx	x								o	xx	o			
193-1188A-9R-1, 5–9 cm	67.65				xxxx												o
193-1188A-10R-1, 39–43 cm	77.69				xxxx							o					
193-1188A-12R-1, 58–61 cm	97.18	xx		xx									xx	xx			
193-1188A-12R-1, 108–111 cm	97.68	xx	x	x									xx	xx	o		
193-1188A-12R-2, 20–24 cm	98.28	xx		x								xx	xx	xx			
193-1188A-13R-1, 8–12 cm	106.38	xx	o	o								o		xx	o		
193-1188A-14R-1, 55–60 cm	116.55				xxxx												
193-1188A-14R-1, 108–111 cm	117.08				xxx	xx											
193-1188A-15R-1, 56–59 cm	126.26	xx							xx			o	xxx	x			
193-1188A-16R-2, 47–51 cm	137.33	xxx		xx					x			x		xx	o		
193-1188A-17R-1, 38–41 cm	145.48	xxx							xx								
193-1188A-18R-1, 78–81 cm	165.08							xxx					xxx	x			
193-1188A-20R-1, 8–12 cm	173.98							xxxx									
193-1188A-20R-1, 68–72 cm	174.58	xxxx		o										o			
193-1188A-21R-1, 21–25 cm	183.31			x				xxx	xx					x	o	xx	
193-1188A-21R-1, 43–47 cm	183.53						xxx	xxx	x								
193-1188A-21R-1, 77–81 cm	183.87						xxx	xxx	x								
193-1188A-21R-1, 142–146 cm	184.52			x				xx	x								
193-1188F-1Z-1, 6–9 cm	218.06	xx		xxxx													
193-1188F-1Z-1, 28–31 cm	218.28	xx		xxxx													
193-1188F-1Z-2, 43–46 cm	219.63	xxx		xxx													
193-1188F-1Z-3, 84–87 cm	221.24																
193-1188F-1Z-4, 17–20 cm	221.77																
193-1188F-2Z-1, 69–72 cm	222.19																
193-1188F-3Z-1, 3–8 cm	222.63	xxx		xx						xx (90)							
193-1188F-8Z-1, 23–26 cm	233.33			xxx					xxx (70)								
193-1188F-6Z-2, 42–45 cm	234.76			xx				xxx		xx (65)							
193-1188F-7Z-1, 50–53 cm	235.5			xxx					xxx (70)								
193-1188F-9Z-1, 35–38 cm	238.05			x					xxx (65)								
193-1188F-13Z-1, 99–102 cm	242.39	x		xxx						x (40)							
193-1188F-14Z-1, 60–63 cm	246.5																
193-1188F-16Z-1, 138–141 cm	256.28			xxxx								o					
193-1188F-16Z-1, 13–17 cm	264.03			xxxx													
193-1188F-23Z-1, 19–22 cm	286.79	xxx		xx						xx (90)							
193-1188F-23Z-2, 25–26 cm	288.35	xxx		xxx								o					
193-1188F-26Z-1, 21–26 cm	300.31	xx		xx						xx (90)		o					
193-1188F-26Z-2, 45–48 cm	301.63	xxx		xx						x (70)							
193-1188F-31Z-1, 37–40 cm	322.97	xxx		xxx								o					
193-1188F-34Z-1, 27–29 cm	336.67	xx		xxx													
193-1188F-34Z-1, 91–94 cm	337.31	xx		xxx								o					
193-1188F-37Z-2, 34–38 cm	346.16	x		xxx										xx			
193-1188F-38Z-2, 86–90 cm	351.15	xx		xx								x		xx			
193-1188F-39Z-2, 27–30 cm	355.19	xx		xxx								o					
193-1188F-41Z-1, 43–46 cm	362.93	xx		xxx								x		xx			
193-1188F-43Z-1, 0–3 cm	371.5	xxx		xxx								x		xx			
193-1188F-43Z-1, 80–83 cm	372.3	xx		xx								x		xx			
193-1188F-44Z-1, 71–74 cm	374.71	xxxx		x								o		x			

a Abbreviations: mbsf = meters below seafloor; Qz = quartz; Cris = cristobalite; Plag = plagioclase; Ill = illite; Pyroph = pyrophyllite; Chl-Sm = chlorite-smectite mixed-layer; Chl-V = chlorite-vermiculite mixed layer; Ill-Sm = illite-smectite mixed-layer; Ill-Chl = illite-chlorite mixed-layer; % III = percentages of illite intertayers in Ill-Sm and Ill-Chi; Py = pyrite; Mag = magnetite; Chl = chlorite; An = anhydrite; xxxx = very abundant (> 90%); xxx = abundant (50–90%); xx = common (5–50%); x = minor (2–5%); o = traces (<2%).

Table 2. Mineralogical assemblagas of the clay fraction (<2 μm) of altered felaic rocks from Hole 1189A (as determined by X-ray diffraction analyses).[a]

Sample	Depth (mbsf)	Chl	Ill	Chl-V	Qz	Cris	Plag	K-fsp
1189A-2R-1, 122–125 cm	10.92	xxx	xxx	o		xx		
1189A-3R-1, 14–17 cm	19.54	xxx		o	o	xx	x	
1189A-4R-1, 14–17 cm	29.24	xxx	x				o	o
1189A-5R-1, 17–20 cm	38.97	xxx	xx				o	
1189A-7R-1, 30–33 cm	58.6	xxx	xx					x
1189A-9R-1, 0–5 cm	77.7	xxx	x		x		xx	
1189A-9R-1, 63–67 cm	78.33	xxx	xx				o	
1189A-10R-1, 77–81 cm	88.07	xxx	xx		x		o	x
1189A-11R-1, 30–33 cm	97.2	xx	xxx					
1189A-12R-1, 83–86 cm	107.33	xxx	xx				o	
1189A-13R-1, 23–33 cm	116.33	xxxx	x				o	

[a] Abbreviations: mbsf = meters below seafloor; Qz = quartz; Cris = cristobalite; Plag = plagioclase; K-fsp = K-feldspar; Ill = illite; Chl-V = chlorite-vermicutite mixed layer.

lite samples from hole 1188A, Al ions make up between 91 and 97% of the octahedral cations and octahedral cation totals lie between 3.95 and 4.04. Alkali and alkaline earth cations are recorded in all pyrophyllite analyses up to a maximum of ~0.5 cations per formula unit (pfu) which is comparable to analyses of well-characterized pyrophyllites given by Newman and Brown (1987).

The structural formula of chlorite in sample 1188A-20R-1, 68–72 cm has 11.0 octahedral cations indicating that it is a trioctahedral chlorite (Foster, 1962). The chlorite in sample 1189A-13R-1, 23–33 cm has a low octahedral cation total of 10.2 indicating a di-, trioctahedral chlorite (Newman and Brown, 1987). The composition of both chlorites is quite variable in terms of Fe and Al in the octahedral sheet but both are ripidolite (Hey, 1954).

Trace element data for the clay concentrates are presented in

Table 3. Mineralogical assemblages of the clay fraction (<2 μm) of altered felsic rocks from Hole 1189B (as determined by X-ray diffraction analyses).[a]

Sample	Depth (mbsf)	Chl	Sm	Ill	Chl-V (% Chl)	Ill-Chl	Ill-V (% Ill)	Qz	Cris	Plag	K-fap	Py
1189B-2R-1, 11–20 cm	40.21	x		xxxx								o
1189B-2R-1, 30–40 cm	40.40	x		xxxx								
1189B-2R-1, 40–50 cm	40.50	xx		xxx								
1189B-3R-1, 68–76 cm	50.38	x		xxxx								
1189B-6R-1, 34–37 cm	79.34	xxx		xx								
1189B-8R-1, 10–14 cm	98.50	xxx		xxx						x		
1189B-8R-1, 70–74 cm	99.10	xxx		x							xxx	
1189B-10R-1, 10–13 cm	118.00	xxx		x							x	
1189B-10R-1, 25–28 cm	118.15	xxx									x	
1189B-10R-1, 40–44 cm	118.30	xxx		x				x		x		
1189B-10R-1, 57–60 cm	118.47	xxx		x				x		x		
1189B-11R-1, 4–7 cm	127.64	xxx		xx			x (90, 70)					
1189B-11R-2, 42–45 cm	128.70	x								xxx	x	
1189B-11R-2, 90–93 cm	129.18						xx (60)		xxx	xx		
1189B-12R-1, 109–112 cm	138.39				xx (60)				xxx	xx	x	
1189B-12R-2, 51–54 cm	139.22						xx (60)		xxx	xx		
1189B-13R-1, 26–28 cm	147.26	xxx		xx							x	
1189B-14R-1, 11–14 cm	156.61	xxx		xx							x	
1189B-14R-1, 115–118 cm	157.65	xxx	x	x							x	
1189B-14R-2, 17–19 cm	157.96	xxx		xx							x	
1189B-15R-1, 128–129 cm	167.36	xx		x		o				xx		
1189B-15R-2, 8–11 cm	167.68	x		o						xx	xx	
1189B-16R-1, 134–137 cm	177.04			o	xx (50)			x		xx	x	
1189B-17R-1, 36–39 cm	185.66	xx		x		o			xx	xx		
1189B-17R-1, 88–91 cm	186.18	xxx		xx		o				xx		
1189B-18R-1, 12–15 cm	195.12	xxx		x						xx	x	
1189B-18R-1, 69–72 cm	195.69	x								xxx	x	
1189B-18R-1, 100–103 cm	196.00	x								xxx	x	
1189B-18R-2, 17–20 cm	196.59	x								xxx	x	
1189B-18R-2, 40–43 cm	196.82	xxx		x						x	o	
1189B-18R-2, 63–66 cm	197.05	xxx		x						x	o	

[a] Abbreviations: mbsf = meters below seafloor; Ill = illite; Chl = chlorite; Chl-V = chlorite-vermiculite mixed layer; Ill-Chl = illite-chlorite mixed layer; Ill-V = illite-vermiculite mixed layer; Qz = quartz; Cris = cristobalite; Plag = plagioclase; K-fsp = K-feldspar; Py = pyrite; % Chl = percentages of chlorite interlayers in Chl-V; % Ill = percentages of illite interlayers in Ill-V.

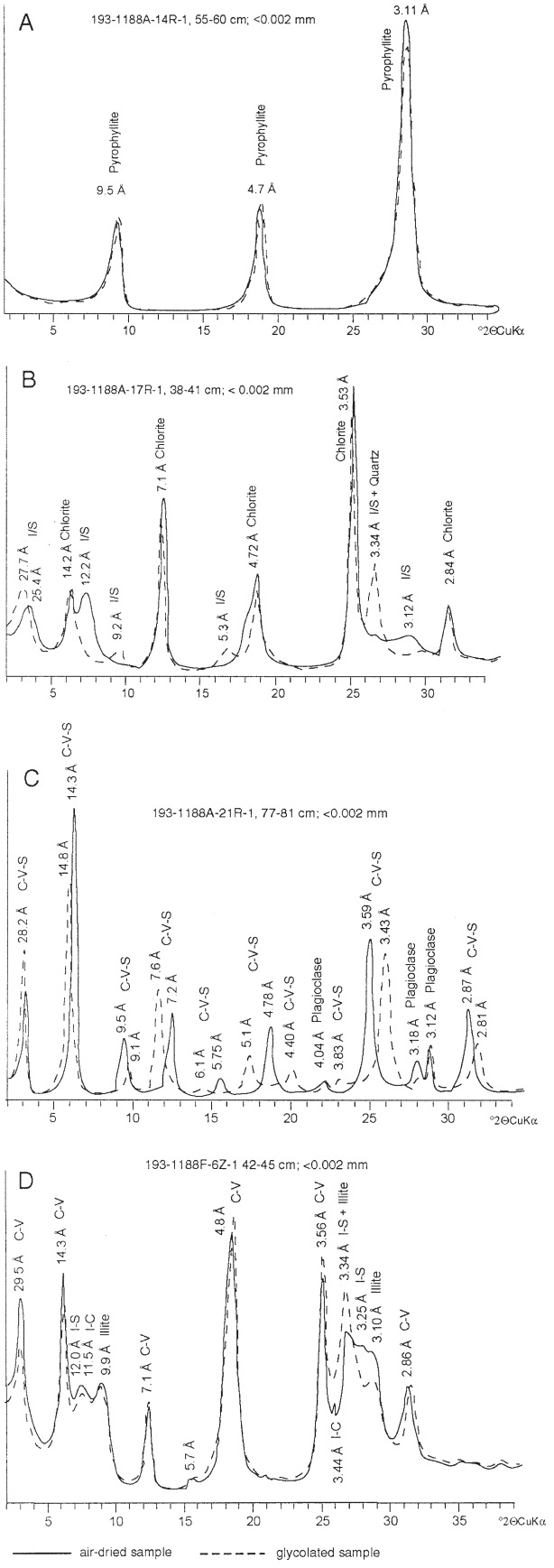

Table 5. REE patterns for these various secondary mineral separates are shown in Figure 4 together with a field for the fresh dacites and rhyodacites from Pual Ridge (Binns, pers. comm.).

$^{87}Sr/^{86}Sr$ ratios of clay concentrates from Holes 1188A and F (Snowcap) vary systematically with depth between 0.7043 and 0.7064 (Table 6, Fig. 5). The lowest ratios are found between 100–200 mbsf where two clay samples, a pyrophyllite and a chlorite, have ratios that are less than that of the present-day black smoker fluid. Below 200 m, the isotope ratios increase to a high >0.706 before falling back to ca. 0.705 near the base of Hole 1188F. Chlorite and illite concentrates from Site 1189 (Roman Ruins) have slightly elevated $^{87}Sr/^{86}Sr$ compositions (0.70410–0.70421) compared to the fresh dacites of the Pual Ridge.

5. DISCUSSION

5.1. Alteration Temperatures

Formation temperatures have been calculated from oxygen isotope data for 12 clay concentrates (Table 7) using published fractionation factors for water-mineral pairs: chlorite-water fractionation from Wenner and Taylor (1971); illite-water fractionation from Sheppard and Gilg (1996); and pyrophyllite-water fractionation from Savin and Lee (1988). An effect of trace contaminants is negligible for temperature calculations. Beside issues concerning the applicability of mineral-water isotopic equilibria (e.g., Savin and Lee, 1988; Sheppard and Gilg, 1996, Cole and Ripley, 1998; Cole et al., 1998) the major source of uncertainty in the temperature calculations is the unknown oxygen isotope value of the hydrothermal fluid with which the minerals equilibrated. Because the oxygen isotope composition of the PACMANUS fluids has not been determined, we have calculated temperatures using a range of possible $\delta^{18}O$ values including pure seawater $\delta^{18}O = 0.0‰$, DESMOS (for location see Fig. 1) fluid $\delta^{18}O = +0.3‰$ (Gamo et al., 1997), and hydrothermal fluid $\delta^{18}O = +1.9‰$ (Shanks et al. 1995). However, from comparison of the oxygen isotopic temperature calculations of mineral formation with temperatures estimated from fluid inclusion studies (255–350°C at Roman Ruins and 270–385°C at Snowcap; Vanko et al., 2004) the lower temperatures derived using the seawater or DESMOS fluids yield more appropriate clay mineral precipitation temperatures at PACMANUS, and these are the values discussed below.

Two concentrates containing I-S (70% illite layers) plus illite have $\delta^{18}O$ values of 4.7 ‰. The fractionation factor for oxygen isotope exchange between I-S clays and water is a function of temperature as well as of the percentage of illite (Savin and Lee, 1988)

$$1000 \ln \alpha_{I/S\text{-}W} = (2.58 - 0.19 f_{Ill}) 10^6 / T^2 - 4.19$$

Fig. 3. XRD patterns (CuK_α) of < 2 μm-size fractions, $MgCl_2$ solvated and $MgCl_2$ + glycolated solvated (= Mg glycerol) for (A) pyrophyllite, (B) illite-smectite (I/S) mixed-layer clay + chlorite + quartz, (C) chlorite-vermiculite-smectite (C-V-S) mixed-layer clay + plagioclase, and (D) chlorite-vermiculite (C-V) mixed-layer clay + illite-smectite (I-S) mixed-layer clay + illite-chlorite (I-C) mixed layer clay + illite.

Table 4. Representative electron microprobe analyses and calculated formulae for phyllosilicates from Sites 1188 and 1189.*

Sample	1188A-9R-1, 5–9 cm	1188A-10R-1, 39–43 cm	1188A-14R-1, 55–60 cm	1188A-20R-1, 68–72 cm	1188F-6Z-1, 23–26 cm	1188F-7Z-1, 50–53 cm	1188F-16Z-1, 138–141 cm	1188F-18Z-1, 13–17 cm	1189A-13R-1, 23–33 cm	1189B-2R-1, 11–20 cm	1189B-10R-1, 25–28 cm
Depth (mbsf = meters below seafloor)	67.65	77.69	116.55	174.58	233.33	235.5	256.28	264.03	116.33	40.21	118.15
Mineral	Pyrophyllite	Pyrophyllite	Pyrophyllite	Chlorite	Illite + Illite-Smectite	Illite	Illite	Illite	Chlorite	Illite	Chlorite
Element (wt%)											
SiO_2	67.9	64.5	61.8	33.6	48.4	54.6	53.1	48.3	33.6	44.4	37.2
TiO_2	1.08	0.64	0.71	0.9	0.50	0.84	0.54	0.08	1.58	0.54	1.20
Al_2O_3	27.3	28.6	30.8	18.0	28.1	31.1	32.7	28.9	20.3	24.0	18.9
FeO	0.12	0.18	0.52	17.5	0.33	0.4	0.25	0.24	8.5	3.1	6.7
MnO	0.01	0.02	0.01	0.23	0.01	0.02	0.00	0.00	0.09	0.02	0.23
MgO	0.47	0.36	0.55	17.6	1.06	1.1	0.92	0.86	17.2	3.9	13.6
CaO	0.08	0.03	0.05	0.34	0.04	0.15	0.07	0.00	1.17	0.24	1.65
Na_2O	0.60	0.86	1.24	0.65	0.60	0.98	1.26	1.10	0.53	0.22	1.13
K_2O	0.25	0.61	1.24	0.12	4.3	4.4	3.9	3.2	1.17	6.8	1.88
Sum	*97.8*	*95.8*	*97.0*	*89.0*	*83.4*	*93.5*	*92.7*	*82.6*	*84.2*	*84.1*	*82.5*
Cations	22-oxygens	22-oxygens	22-oxygens	28-oxygens	22-oxygens	22-oxygens	22-oxygens	22-oxygens	28-oxygens	22-oxygens	28-oxygens
Si	7.98	7.77	7.45	6.59	6.98	7.01	6.85	6.97	6.68	6.73	7.36
Al IV	0.02	0.23	0.55	1.41	1.02	0.99	1.15	1.03	1.32	1.27	0.64
Sum tet.	*8.00*	*8.00*	*8.00*	*8.00*	*8.00*	*8.00*	*8.00*	*8.00*	*8.00*	*8.00*	*8.00*
Al VI	3.76	3.84	3.83	2.76	3.76	3.72	3.82	3.89	3.44	3.02	3.77
Tl	0.10	0.06	0.06	0.13	0.05	0.08	0.05	0.01	0.23	0.08	0.18
Fe	0.01	0.02	0.05	2.88	0.04	0.04	0.03	0.03	1.41	0.39	1.11
Mn	0.00	0.00	0.00	0.04	0.00	0.00	0.00	0.00	0.02	0.00	0.04
Mg	0.08	0.06	0.10	5.15	0.23	0.21	0.18	0.19	5.11	0.88	4.01
Sum oct.	*3.95*	*3.96*	*4.04*	*10.96*	*4.08*	*4.05*	*4.08*	*4.12*	*10.21*	*4.25*	*9.11*
Ca	0.01	0.00	0.01	0.07	0.01	0.02	0.01	0.00	0.25	0.04	0.35
Na	0.14	0.20	0.30	0.25	0.17	0.24	0.32	0.31	0.20	0.08	0.43
K	0.04	0.10	0.20	0.04	0.8	0.71	0.65	0.58	0.30	1.27	0.47
Sum of cations	*12.14*	*12.26*	*12.55*	*19.33*	*13.08*	*13.03*	*13.07*	*13.01*	*18.96*	*13.73*	*18.36*

* The structural formulae for the pure pyrophyllite and illite samples were calculated on the basis of 22 oxygens whereas formulae for the chlorite samples were calculated on the basis of 28 oxygens.

Table 5. Trace element analyses of hydrothermal clay minerals from Snowcap (Site 1188) and Roman Ruins (Site 1189).[a]

Element	1188A-7R-1 144–148 cm Pyrophyllite	1188A-9R-1 5–9 cm Pyrophyllite	1188A-10R-1 39–43 cm Pyrophyllite	1188A-14R-1 55–60 cm Pyrophyllite	1188A-20R-1 68–72 cm Chlorite	1188F-7Z-1 50–53 cm Illite/I-S	1188F-18Z-1 138–141 cm Illite	1188F-18Z-1 13–17 cm Illite	1189A-13R-1 23–33 cm Chlorite	1189B-2R-1 30–40 cm Illite	1189B-10R-1 25–28 cm Chlorite	BHVO-2 certified	±	BHVO-2 measured Mean*	BHVO-2 Std Dev	BHVO-2 Rel Std Dev
Sc	20.0	20.6	21.0	21.8	35.8	21.7	n.d.	11.4	38.8	20.1	27.5	32	1.0	29.1	1.67	5.8
V	48.8	49.0	50.3	13.1	334	65.3	199.7	76.1	369	76.8	371	317	11.0	315	8.1	2.6
Cr	26.7	32.7	45.8	4	125	13.2	69.1	23.7	169	51.9	113	280	19.0	270	0.62	0.2
Co	3.9	0.17	0.30	0.88	0.61	1.40	1.01	0.33	17.1	10.5	1.00	45	3.0	42.3	0.66	1.6
Nl	11.8	5.0	17.8	13.4	18.8	12.5	15.7	8.4	47.5	122	37.2	119	7.0	109	3.5	3.2
Cu	60.4	54.4	61.9	94.8	78	44.8	61.4	102	295	1051	278	127	7.0	117	1.77	1.5
Zn	21.5	22.4	34.4	26.6	107	33.8	70.4	38.7	106	308	548	103	6.0	94.7	10.7	11.3
Ga	23.7	13.9	11.9	22.5	50.9	19.0	35.0	9.5	38.6	50.1	28.8	21.7	0.9	20.2	1.19	5.9
Rb	18.2	11.0	3.1	29.9	19.7	27.8	23.8	24.9	2.3	111	15.8	9.8	1.0	9.4	0.31	3.3
Sr	54.1	93.7	22.9	260	370	243	307	111	90.2	20.1	91.9	389	23.0	382	27.2	7.1
Y	45.4	41	26.8	30.7	28.0	37.4	32.7	27.5	33.1	55.0	40.4	26	2.0	25.5	1.41	5.5
Zr	217	152	192	130	97.3	65.0	81.2	274	33.5	199	149	172	11.0	166	5.8	3.5
Nb	2.8	2.4	2.5	1.62	1.30	1.56	1.43	0.91	0.92	1.70	1.60	*18*	*2.0*	18.5	1.10	5.9
Ca	0.88	0.61	0.49	0.72	0.51	0.5	n.d.	0.87	0.73	8.2	0.91			0.1	0.03	28.0
Ba	402	398	13.1	371	278	1456	867	3769	38.3	1539	2741	130	13.0	132	5.9	4.5
Hf	6.2	4.8	5.8	3.8	2.8	2.6	2.7	10.5	1.52	5.7	5.3	4.1	0.3	4.9	0.04	0.8
Pb	3.8	7.0	3.3	6.7	4.3	4.6	n.d.	3.6	3.0	131	27.1			1.9	0.42	22.7
Th	2.3	1.99	2.1	1.38	0.94	2.3	1.62	4.6	1.02	2.8	2.5	*1.2*	*0.3*	1.6	0.06	3.9
U	6.8	0.88	0.91	0.80	0.52	0.93	0.73	2.3	0.47	5.9	1.50			0.5	0.02	3.5
La	11.3	8.4	10.4	10.8	8.8	16.9	12.9	22.3	8.3	39.2	15.8	15	1.0	15.5	0.55	3.6
Ce	29.7	20.9	21.5	25	20.9	49.8	35.4	35.7	20.3	113.7	35.7	38	2.0	38.4	1.26	3.3
Pr	4.9	2.9	2.7	3.6	3.0	6.2	4.6	4.3	2.9	15.5	5.2			5.5	0.26	5.1
Nd	25.2	13.4	11.3	15.4	13.9	28.2	21.1	15.8	13.8	74.8	25.8	25	1.8	25.7	1.03	4.0
Sm	7.2	4.4	2.6	4	3.8	7.3	5.6	2.7	3.6	19.1	6.9	*6.2*	*0.4*	6.4	0.43	6.7
Eu	1.55	1.21	0.72	1.12	1.23	2.3	1.77	1.80	0.57	8.7	2.3			2.1	0.11	5.3
Gd	7.3	5.7	2.5	4.2	4.1	8.4	6.3	2.8	4.2	17.3	8.0	*6.3*	*0.2*	6.6	0.20	3.0
Tb	1.20	1.04	0.47	0.73	0.69	1.40	1.05	0.54	0.73	2.4	1.30	*0.9*		1.0	0.04	4.3
Dy	7.6	8.7	3.6	4.6	4.6	9.0	6.8	4.0	5.1	12.5	8.2			5.6	0.24	4.2
Ho	1.65	1.42	0.93	1.06	1.00	1.90	1.45	1.10	1.14	2.4	1.80	*1.04*	*0.04*	1.1	0.04	4.1
Er	4.9	4.1	3.3	3.2	3.0	5.9	4.5	4.3	3.4	6.8	5.7			2.8	0.15	5.4
Tm	0.75	0.6	0.58	0.5	0.45	0.92	0.69	0.80	0.52	1.03	0.85			0.4	0.02	5.3
Yb	5.2	4.1	4.3	3.5	3.1	6.5	4.8	6.2	3.5	6.5	5.6	*2*	*0.2*	2.2	0.08	3.8
Lu	0.82	0.63	0.73	0.5	0.54	0.99	0.77	1.10	0.52	1.10	0.87	*0.28*	*0.0*	0.3	0.01	4.8
Nd_N/Yb_N	1.8	1.2	1.0	1.8	1.6	1.8	1.8	0.9	1.4	4.2	1.7					
Eu^*_N	41.4	28.2	14.6	23.3	22.4	44.3	33.4	15.7	22.0	104.9	42.0					
Eu/Eu^*_N	0.62	0.71	0.82	0.80	0.91	0.88	0.88	1.91	0.43	1.06	0.91					

[a] BHVO-2 = international reference standard, analyzed during the ICP-MS analytical runs, for controlling accuracy of analytical results; trace elements analyzed by ICP-MS; concentrations of trace elements expressed in ppm.

* Number of standard samples: 4; Std Dev = Standard Deviation; Rel Std Dev = Relative Standard Deviation

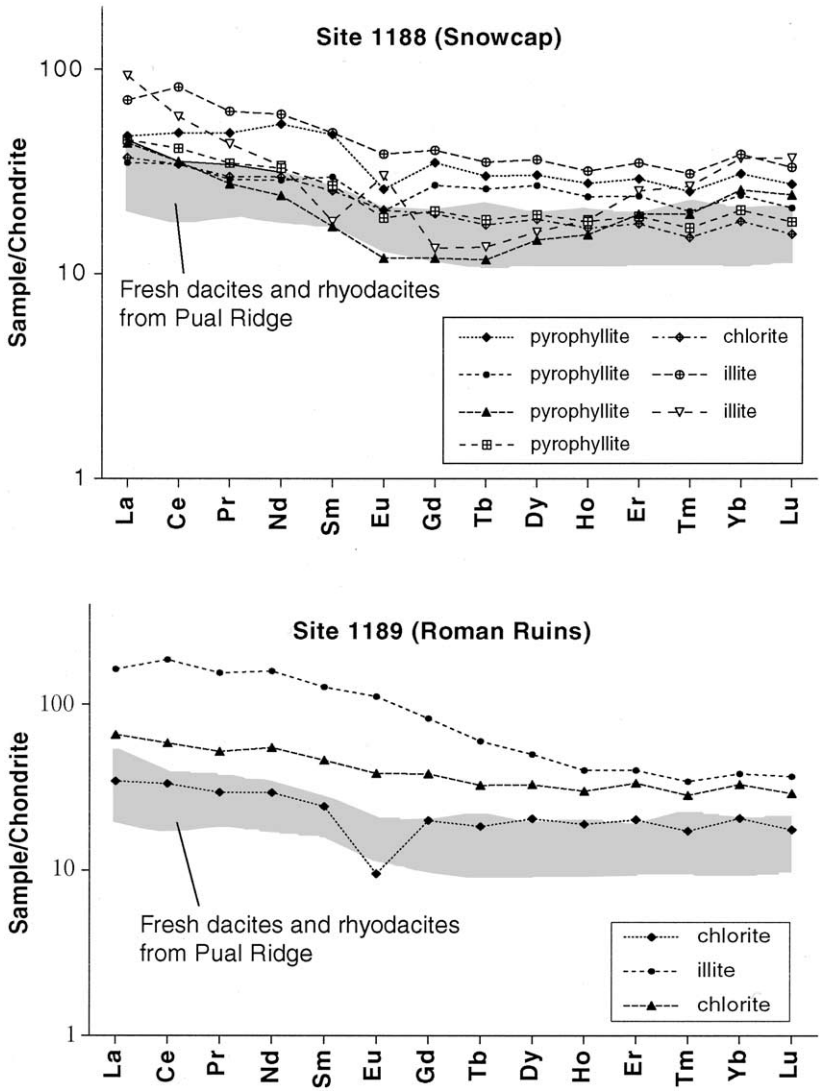

Fig. 4. Chondrite-normalized rare earth element patterns of clay samples from Holes 1188A, 1188F, 1189A and 1189B; normalizing values are from Sun and McDonough (1989). Field for rare earth element pattern of unaltered dacites and rhyodacites from Pual Ridge (R. Binns, unpublished data).

where $\alpha_{I/S-W}$ is the fractionation factor for oxygen isotope exchange between I-S mixed-layer and water, f_{Ill} is the fraction of illite layers in the I-S, and T is temperature in Kelvin.

Temperatures were calculated for these two samples assuming 50% of the volume of both is illite and the other 50% is I-S. Using illite-water and I/S-water fractionation equations and preferring the seawater fluid composition, we calculate a formation temperature of 250°C in Hole 1188F (Fig. 6). The isotopic compositions of secondary illites below 250 mbsf in Hole 1188F give formation temperatures between 250° and 300°C. In Hole 1188A, pyrophyllite and chlorite yield temperatures of 260° to 310°C and 225°C, respectively (Fig. 6, Table 7).

The calculated temperature for a pure chlorite in Hole 1189A at 116 mbsf is 250°C (Fig. 6). A pure illite at 40 mbsf in Hole 1189B formed at a calculated temperature of 305°C, whereas chlorites from the lower sequence (118 and 197 mbsf) show formation temperatures of 235°C and 220°C, respectively.

In addition, quartz formation temperatures have been calculated using the quartz-water fractionation factor of Knauth and Epstein (1976). Here too, if we were to use the $\delta^{18}O$ of +1.9‰ for the hydrothermal fluid proposed by Shanks et al. (1995) we would compute an unrealistically high mineral formation temperature of $>$ 500°C leading us to favor lower $\delta^{18}O$ values for the PACMANUS fluids.

The oxygen isotope ratios of quartz separates from crosscutting veins of two samples of Hole 1189A give formation temperatures of 350°C at ~58.5 mbsf (Fig. 6). Interestingly, the higher oxygen isotope fractionation temperature of 400°C was estimated from a vein quartz sample at ~ 40 mbsf just below an interval with massive to semimassive sulfides. A decrease in temperature with depth is indicated by a higher $\delta^{18}O$ value of a vein quartz sample at ~80 mbsf.

Table 6. Strontium isotopic compositions and strontium concentrations of hydrothermal clay minerals from Snowcap and Roman Ruins.

Sample	Depth (mbsf)	Mineral	$^{87}Sr/^{88}Sr$	Stat Error	Sr (ppm)	1/Sr
193-1188A-7R-1, 144–148 cm	49.64	Pyrophyllite	0.705861	0.000008	54.1	0.018
193-1188A-9R-1, 5–9 cm	67.65	Pyrophyllite	0.705368	0.000004	93.7	0.011
193-1188A-10R-1, 39–43 cm	77.69	Pyrophyllite	0.705458	0.000006	22.9	0.044
193-1188A-14R-1, 55–60 cm	116.55	Pyrophyllite	0.704557	0.000007	260	0.0038
193-1188A-20R-1, 68–72 cm	174.58	Chlorite	0.704298	0.000003	370	0.00270
193-1188F-6Z-1, 23–26 cm	233.33	Illite, Ill-Sm	0.705457	0.000003	n.d.	n.d.*
193-1188F-7Z-1, 50–53 cm	235.5	Illite, Ill-Sm	0.705527	0.000003	243	0.0041
193-1188F-18Z-1, 138–141 cm	256.28	Illite	0.706398	0.000003	306	0.0033
193-1188F-18Z-1, 13–17 cm	264.03	Illite	0.706178	0.000004	111	0.009
193-1188F-34Z-1, 91–94 cm	337.31	Illite	0.705633	0.000004	n.d.	n.d.
193-1188F-39Z-2, 27–30 cm	355.19	Illite	0.705095	0.000003	n.d.	n.d.
193-1189A-13R-1, 23–33 cm	116.33	Chlorite	0.704001	0.000003	90.2	0.0111
193-1189B-2R-1, 30–40 cm	40.40	Illite	0.704100	0.000034	20.1	0.0497
193-1189B-10R-1, 25–28 cm	118.15	Chlorite	0.704215	0.000003	91.9	0.0109

* n.d. = no data.

5.2. Zonation of Alteration Characteristics

Throughout the PACMANUS hydrothermal field, the appearance, composition and abundance of the main secondary phases vary both laterally and vertically. This alteration heterogeneity reflects a variable interaction between the felsic crust and a hydrothermal fluid under changing physical and/or chemical conditions.

5.2.1. Snowcap

Based on variations in alteration style and secondary mineralogy as well as isotopic temperatures, five different alteration zones have been distinguished at the Snowcap site:

5.2.1.1. Zone 1. A zone from ~50 to 120 mbsf is characterized by a chlorite ± illite-cristobalite-plagioclase assemblage intercalated with a monomineralic pyrophyllite assemblage. Studies of the style and mineralogy of the altered rocks indicate that a chlorite ± illite-cristobalite-plagioclase alteration is overprinted locally by pyrophyllite alteration (Binns et al., 2002). Based on oxygen isotope data the pyrophyllite formation occurred between 260° and 310°C. The fluid inclusion record from shallow samples (below 100 mbsf) contains evidence for the previous existence of a range of both moderate-temperature (e.g., ≥150°C) and high-temperature (e.g., up to 320°C) fluids suggesting complex overprinting relationships (Vanko et al., 2004). The presence of intensely veined and fractured breccias suggests that this zone has

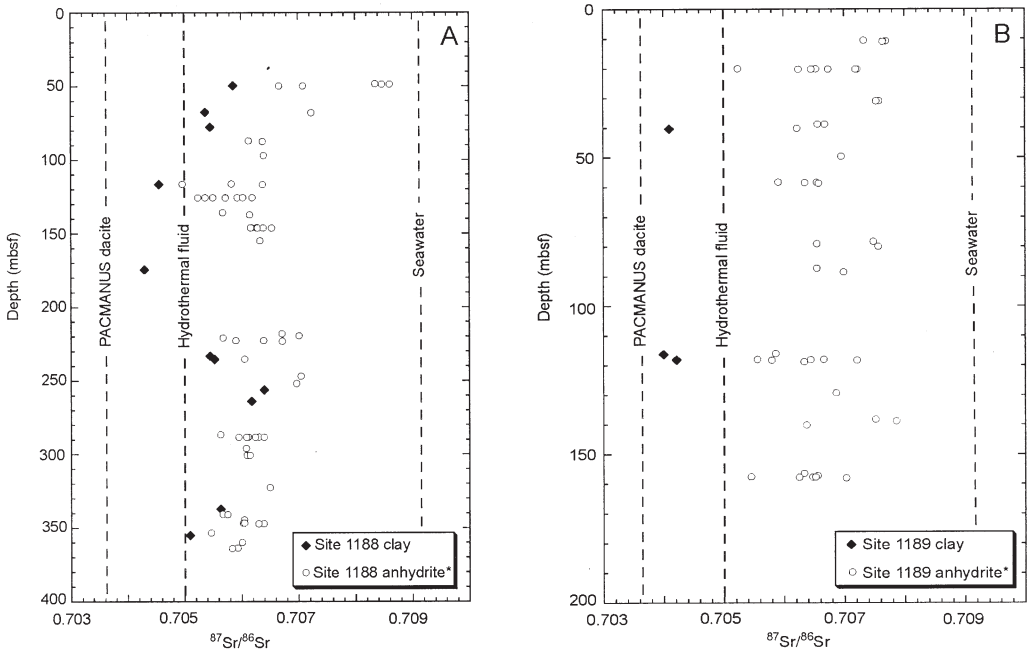

Fig. 5. Plots showing the Sr-isotopic ratio of anhydrite veins as a function of depth (Roberts et al., 2003), compared to Sr-isotopic ratios of secondary clay minerals vs. depth (this study). A. Sr isotopic ratios for Snowcap (Site 1188). B. Sr-isotopic ratios for Roman Ruins. $^{87}Sr/^{86}Sr$ ratio for PACMANUS dacite is from R. Binns (unpublished data); $^{87}Sr/^{86}Sr$ ratio for the end-member hydrothermal fluid is from Douville (1999).

Table 7. Oxygen isotope ratio and calculated mineral formation temperature of clay and quartz samples from PACMANUS hydrothermal field.

Sample	Depth (mbsf)	Mineral	Interlayered illite (%)	$\delta^{18}O$	Isotopic temperature (°C) Fluid $\delta^{18}O$: 0.0*	Isotopic temperature (°C) Fluid $\delta^{18}O$: 0.3†	Isotopic temperature (°C) Fluid $\delta^{18}O$: 2.0§
193-1188A-9R-1, 5–9 cm	67.65	Pyrophyllite		6.4	260	265	320
193-1188A-10R-1, 39–43 cm	77.69	Pyrophyllite		4.8	305	310	380
193-1188A-14R-1, 55–60 cm	116.55	Pyrophyllite		4.7	310	315	380
193-1188A-20R-1, 68–72 cm	174.58	Chlorite		1.6	225	235	330
193-1188F-6Z-1, 23–26 cm	233.33	Illite, Ill-Sm	70	4.7	250	260	325
193-1188F-7Z-1, 50–53 cm	235.50	Illite, Ill-Sm	70	4.7	250	260	325
193-1188F-16Z-1, 138–141 cm	256.28	Illite		4.7	260	270	335
193-1188F-18Z-1, 13–17 cm	264.03	Illite		5.0	250	260	320
193-1188F-34Z-1, 91–94 cm	337.31	Illite		3.5	300	310	400
193-1188F-39Z-2, 27–30 cm	355.19	Illite		3.8	290	300	380
193-1189A-7R-1, 19–23 cm	58.49	Quartz		4.6	350	365	450
193-1189A-7R-1, 24–26 cm	58.54	Quartz		4.5	355	370	460
193-1189A-13R-1, 23–33 cm	116.33	Chlorite		1.0	250	265	375
193-1189B-2R-1, 10–20 cm	40.20	Quartz		3.5	400	415	530
193-1189B-2R-1, 30–40 cm	40.40	Illite		3.4	305	315	410
193-1189B-6R-1, 45–56 cm	79.45	Quartz		4.1	370	385	485
193-1189B-10R-1, 25–28 cm	118.15	Chlorite		1.3	235	250	350
193-1189B-18R-2, 40–43 cm	196.82	Chlorite		1.8	220	230	315

* Seawater composition.
† DESMOS fluid composition (Gamo et al., 1997).
§ hydrothermal fluid (Shanks et al., 1995).

layers of higher permeability. The occurrence of pyrophyllite suggests interaction of the felsic rocks with fluids of low pH (<3) (Yeats et al., 2001).

5.2.1.2. Zone 2. Between 126 and 185 mbsf, chlorite and chlorite-vermiculite, chlorite-smectite and illite-smectite mixed-layer phases are the main phyllosilicate assemblages suggesting a fairly high pH fluid (>5) (Yeats et al., 2001). A chlorite formation temperature of 230°C was calculated from oxygen isotope data. This is compatible with the presence of chlorite mixed-layer phases, whose stability range has been shown to be < 250°C (e.g., Inoue et al., 1987; Schiffman and Fridleifsson, 1991; Lackschewitz et al. 2000a).

5.2.1.3. Zone 3. Rocks between 218 and 222 mbsf exhibit only chlorite and illite as the secondary phyllosilicate assemblage indicating slightly higher temperatures than in zone 2.

5.2.1.4. Zone 4. From 222 to 302 mbsf, the alteration style is similar to zone 2, but chlorite-smectite mixed-layer phases are lacking whereas illite-smectite mixed-layer phases appear. Oxygen isotope compositions of illite separates suggest formation temperatures of 250 to 260°C, compatible with observations that illite mixed-layers can occur at temperatures up to 270°C (Yeh and Savin, 1977).

5.2.1.5. Zone 5. Below 322 mbsf, chlorite and illite are always observed together, whereas mixed layer phases disappear indicating alteration at higher (290–300°C) temperature.

5.2.2. Roman Ruins

In terms of the phyllosilicate assemblages, hole 1189A contains a quite uniform chlorite-illite alteration at formation temperatures of ~250°C over the whole sequence. Cristobalite becomes totally replaced by quartz below 25 mbsf (Shipboard Scientific Party, 2002). Cristobalite typically forms at temperatures ≤150°C (Kear, 1989; Corbett and Leach, 1998), whereas our calculated quartz formation temperatures of 350°C indicate that an early "chloritic-illitic" alteration is overprinted by a high-temperature vein-related quartz formation.

The sequence and conditions of alteration in hole 1189B can be divided into four different alteration zones on the basis of secondary clay mineral composition and isotopic temperatures.

5.2.2.1. Zone 1. In the uppermost zone from 40 to 80 mbsf illite ± chlorite formed at temperatures of ~ 300°C. Coarse-grained quartz in cross-cutting veins formed at temperatures between 370° and 400°C suggesting later intrusion of silica-rich, high-temperature hydrothermal fluids.

5.2.2.2. Zone 2. From 98 to 120 mbsf, chlorite ± illite occur together with plagioclase and K-feldspar. Chlorite formed at temperatures of 235°C.

5.2.2.3. Zone 3. Between 125 and 190 mbsf, chlorite, illite and chlorite-vermiculite, illite-chlorite and illite-vermiculite mixed-layer phases are the main phyllosilicate assemblages indicating lower formation temperatures than for the zones below and above.

5.2.2.4. Zone 4. Below 195 mbsf chlorite ± illite occur together with plagioclase and K-feldspar. Chlorite formed at temperatures of 220°.

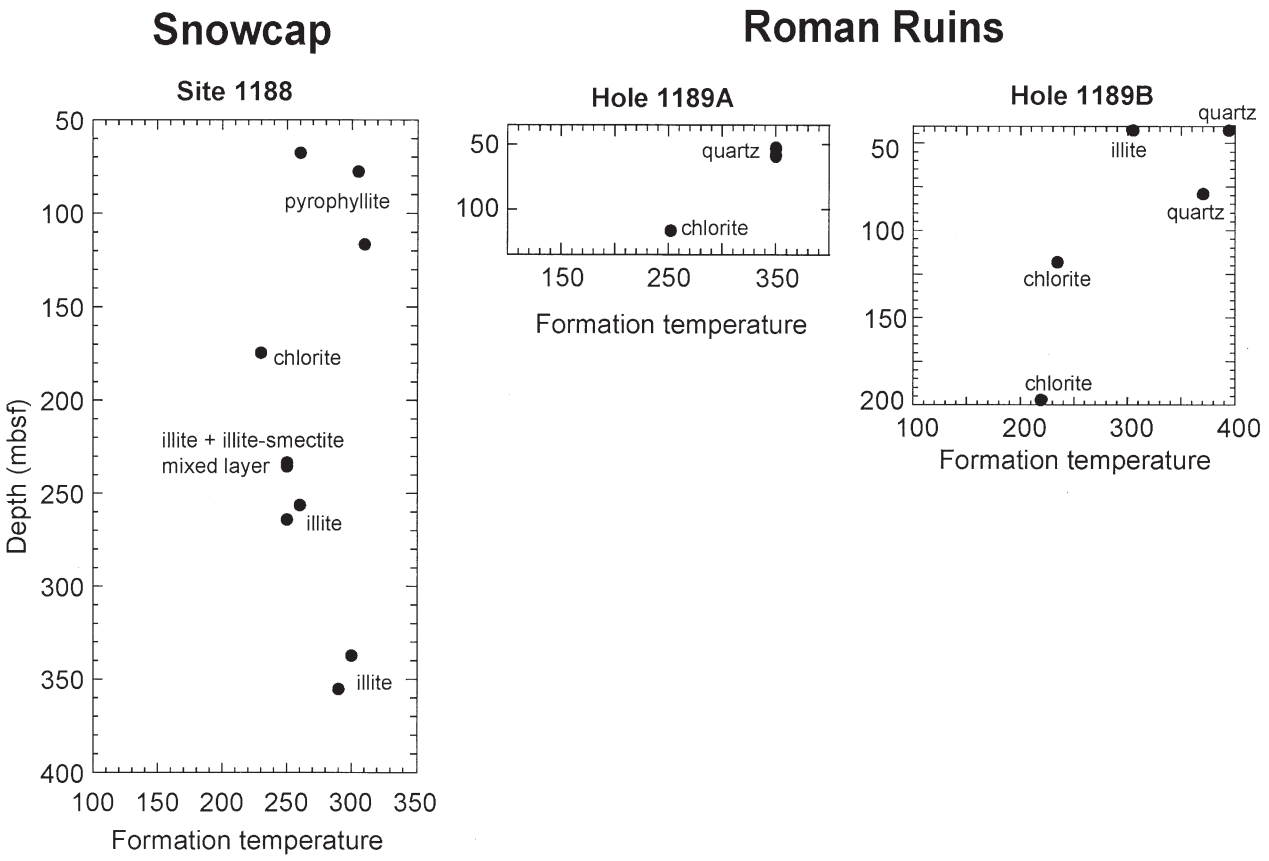

Fig. 6. Downhole variation of oxygen isotope formation temperatures of secondary clay minerals in Holes 1188A, F, 1189A and 1189B. We have calculated formation temperatures using a pure seawater $\delta^{18}O$ value of 0.0‰ (see "Discussion" for details).

5.3. Compositional Effects of Alteration

5.3.1. Comparisons of Fresh and Altered Bulk Rocks

To derive alteration-related chemical mass changes for various elements we have performed major and trace element analyses on some clay-rich bulk rock samples (Table 8) and compared them to modeled precursors. The compositions of the precursors were derived using algorithms developed from CSIRO Exploration and Mining's unpublished database of more than 70 fresh lava samples from Pual Ridge (Yeats and Binns, pers. comm.). Using these data, Yeats and Binns have constructed well constrained fractionation trends relating the concentration of individual elements to Zr/TiO_2, a ratio that is not changed during alteration at the PACMANUS site. These fractionation trends allow a precursor concentration for each element of interest to be calculated for any altered sample with a known Zr/TiO_2 ratio. Typically, scatter of the fractionation trends is low and it is estimated that the error in calculated element precursor element concentration generated by using this methodology is of the order of 5% relative.

The calculation of chemical changes is based on the method of Gresens (1967) which was later modified by Grant (1986) in which the concentration of a component in the altered rock is compared to that in the original through a mass change term

$$C_i^A = M^O/M^A(C_i^O + \Delta C_i)$$

in which C_i^A = concentration of component i in the altered rock; M^O = mass of the original, fresh rock; M^A = mass of the altered rock; C_i^O = concentration of component i in the parent rock; and ΔC_i = change in concentration of component i. Results for elements from individual samples are plotted as C_i^A vs. C_i^O, where all data points lie along an arc of a circle centered on the origin. By evaluating which points group together, it is possible to evaluate which elements to use for calculation of the mass change term (M^O/M^A), which can then be used to calculate elemental gains and losses.

A comparison of the magnitudes and directions of major element oxide and trace element fluxes for three alteration styles (i.e., chloritization, illitization, and silica-pyrophyllite alteration (bleaching) of felsic volcanics) allows us to indicate the elemental gains and losses during each step of the alteration sequence. Figure 7 shows results of the mass-transfer calculations, with positive values indicating a percent gain and negative values indicating a percent loss.

1. Chloritization of fresh rocks by reactions with a hydrothermal fluid-seawater mixture resulted in distinct uptake of Fe_2O_3, MgO, Co, Cr, Eu, Pb and V. Large proportions of K_2O, Ba, Cu, Rb, Th, Tl and U were lost from the rock.

2. Illitization of the rock has resulted in an 800-percent enrichment of Ba and a 300-percent enrichment in Cr. Slight enrichments in Al_2O_3, K_2O, Hf, La, Th, and U are also calcu-

Table 8. Chemical compositions of strongly altered bulk rock samples compared to that in the calculated fresh precursors through a mass change term (M^o/M^A), which we have used to calculate the average percent change (%Δ) in samples from different alteration zones.*

Element	1188A-9R-1 5–9 cm altered with pyrophillite	1188A-9R-1 5–9 cm precursor	(%Δ) with M^o/M^A = 0.9708	1188A-10R-1 39–43 cm altered with pyrophillite	1188A-10R-1 39–43 cm precursor	(%Δ) with M^o/M^A = 0.9198	1188A-14R-1 55–60 cm altered with pyrophllite	1188A-14R-1 55–60 cm precursor	(%Δ) with M^o/M^A = 1.083	1188A-20R-1 68–72 cm altered with chlorite	1188A-20R-1 68–72 cm precursor	(%Δ) with M^o/M^A = 0.8816	1188F-18Z-1 13–17 cm altered with illite	1188F-18Z-1 13–17 cm precursor	(%Δ) with M^o/M^A = 1.487
SiO_2	85.3	67.4	−0.2	72.9	65.6	21	84.4	67.7	−11	55.8	54.9	−25	60.0	64.6	−38
TiO_2	0.61	0.63	−0.5	0.68	0.72	0.3	0.65	0.62	−0.9	0.75	0.85	0.1	1.13	0.76	−0.2
Al_2O_3	13.7	14.1	−0.1	14.3	14.4	8.0	15.5	14.1	3.5	12.8	15.0	−3.2	23.5	14.5	8.6
Fe_2O_3	3.3	5.0	−32	0.99	5.7	−8.1	3.0	4.9	−43	11.8	8.5	102	4.0	6.1	−55
MnO	0.01	0.14	−92	0.01	0.15	−0.3	0	0.14	−100	0.1	0.15	−24	0.0	0.15	−100
MgO	0.18	1.17	−84	0.15	1.48	−89	0.24	1.12	−80	4.8	1.7	220	0.34	1.84	−88
CaO	3.3	3.3	3.8	1.4	3.0	−61	2.4	3.2	−29	2.5	4.5	−37	0.44	4.2	−93
Na_2O	0.88	4.9	−81	0.85	4.8	−81	1.06	4.9	−80	2.7	4.6	−33	1.3	4.7	−81
K_2O	0.16	1.70	−90	0.42	1.54	−70.0	0.75	1.73	−59	0.13	1.48	−90	2.3	1.45	5.8
P_2O_3	0.15	0.14	9.8	0.15	0.19	−13.0	0.08	0.13	−44	0.38	0.28	58	0.13	0.22	−69
Sc	8.4	12.0	−28	7.8	13.4	−37	7.9	11.8	−37	11.5	18.6	−21	11.5	14.3	−46
V	24.4	28.5	−12	25.1	47.2	−42	6.5	26.1	−77	148	77	119	65.2	62.4	−30
Cr	16.3	2.7	512	17.1	3.4	445	2.7	2.8	−2.8	87.1	27.1	284	22.6	3.8	295
Co	5.5	6.2	−7.7	0.30	8.0	−96	5.4	5.9	−13	20.0	12.0	90	7.5	9.2	−45
Nl	7.1	7.1	3.7	3.3	7.6	−53	4.7	7.0	−37	37.7	27.9	53	5.8	7.9	−52
Cu	10.3	22.4	−63	5.1	24.8	−78	4.1	22.0	−82	8.8	48.6	−80	12.4	28.3	−68
Zn	14.1	79.6	−82	72.0	82.6	−5.2	9.0	79.1	−89	33.4	90.0	−58	7.0	84.3	−94
Ga	8.1	15.2	−45	6.6	15.8	−54	11.8	15.1	−26	26.5	18.0	67	8.2	18.1	−66
Rb	1.77	22.4	−92	4.5	20.1	−76	5.48	22.8	−77	0.87	23.9	−98	13.7	18.8	−51
Sr	273	260	0.8	100	307	−64	214	275	−27	226	330	−22	125	323	−74
Y	32.7	29.1	16	23.1	28.0	−11	24.4	29.3	−23	18.0	33.3	−39	8.2	27.4	−80
Zr	111	114	0.8	96.7	104	1	123	115	0.4	17.9	94.0	−0.1	147	88.7	0.2
Nb	1.46	n.d.	n.d.	1.62	n.d.	n.d.	1.85	n.d.	n.d.	0.92	n.d.	n.d.	2.8	n.d.	n.d.
Ca	0.08	0.80	−69	0.10	0.72	−85	0.02	0.81	−97	0.00	n.d.	n.d.	0.14	0.67	−86
Ba	334	326	5.6	523	298	91	428	330	22	71.1	278	−71	3701	283	780
Ta	0.12	n.d.	n.d.	0.12	n.d.	n.d.	0.15	n.d.	n.d.	0.08	n.d.	n.d.	0.23	n.d.	n.d.
Tl	0.25	0.11	−57	0.23	0.11	−48	0.26	0.31	14	0.04	0.34	−89	0.22	0.30	−72
Hf	3.4	3.4	3.4	3.6	3.0	28	4.7	3.4	29	0.88	2.8	−64	5.8	2.8	33
Pb	36.4	5.7	581	39.1	5.4	665	5.2	5.7	−14	11.0	7.0	79	1.91	5.3	−76
Th	1.28	1.28	3.2	1.25	1.16	17	1.91	1.30	−39	0.65	2.2	−68	2.0	1.10	22
U	0.63	0.72	−9.3	0.49	0.65	−17	0.78	0.73	0.5	0.31	1.22	−71	1.36	0.61	50
La	7.7	12.1	−35	9.3	11.2	−9.7	11.0	12.3	−16	7.8	10.2	−13	20.3	10.7	27
Ca	18.9	59.5	−67	21.7	57.7	−59	25.7	59.8	−80	20.6	24.6	−5	34.3	56.7	−59
Pr	3.0	4.0	−23	3.3	3.8	−6.6	4.0	4.1	−8.5	3.4	3.5	9	3.4	3.7	−38
Nd	15.4	17.2	−7.8	15.6	16.4	3.8	17.6	17.4	−4.8	16.2	15.6	17	11.9	16.0	−50
Sm	4.7	4.4	11	4.1	4.2	4.5	4.5	4.4	−4.0	4.3	4.5	8	1.82	4.2	−71
Eu	1.50	1.44	7.6	1.18	1.43	−12	1.08	1.44	−29	0.85	0.48	101	0.82	1.42	−81
Gd	5.23	4.9	10	3.80	4.8	−13	4.42	4.9	−16	3.95	3.2	41	1.30	4.7	−81
Tb	0.81	0.91	3.3	0.68	0.88	−18	0.76	0.91	−22	0.82	0.86	−18	0.26	0.86	−80
Dy	6.4	5.4	20	4.6	5.3	−1.0	5.3	5.5	−8.1	4.2	5.4	−12	2.3	5.2	−70
Ho	1.35	1.26	10	1.03	1.21	−7.8	1.14	1.27	−15	0.01	1.18	−12	0.86	1.19	−63
Er	4.2	3.8	22	3.4	3.5	5.9	3.8	3.6	−5.9	2.5	3.7	−22	2.7	3.4	−48
Tm	0.64	0.59	11	0.58	0.56	13	0.57	0.59	−10	0.36	0.63	−35	0.51	0.54	−37
Yb	4.5	3.8	22	3.6	3.6	9.2	3.7	3.8	−9.7	2.4	3.5	−21	4.2	3.5	−19
Lu	0.65	0.69	−3.5	0.54	0.64	−9.6	0.60	0.70	−19	0.35	0.53	−26	0.67	0.62	−27

* Concentrations of all oxides expressed in wt %; concentrations of trace elements are expressed in ppm. n.d. = no data

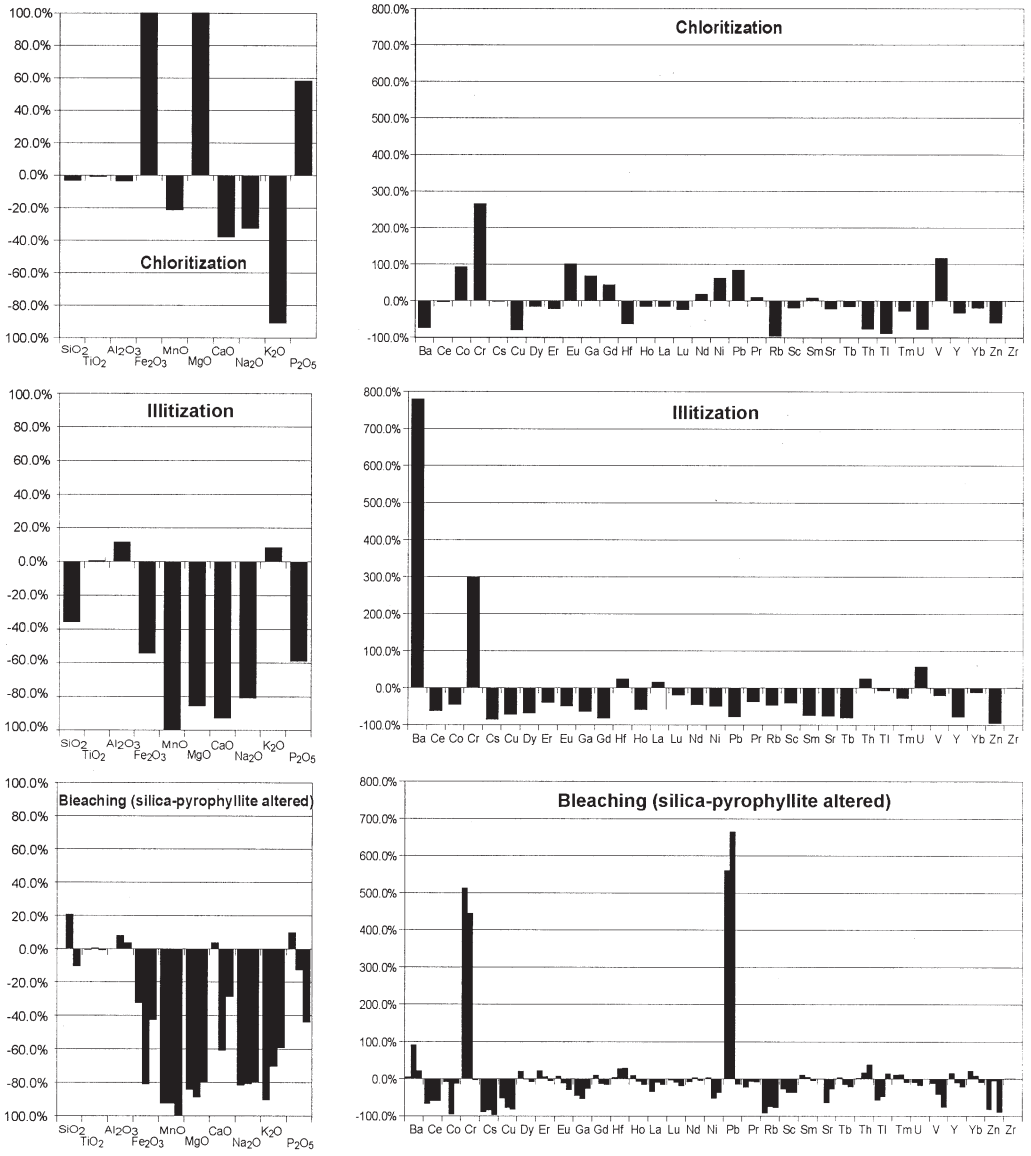

Fig. 7. Relative gains and losses of major and trace elements calculated for the sequence of hydrothermal alteration of felsic lava flows in the active PACMANUS site. Sample 1188A-20R-1, 68–72 cm = chloritization; sample 1188F-18Z-1, 13–17 cm = illitization; samples 1188A-9R-1, 5–9 cm, 1188A-10R-1, 39–43 cm and 1188A-14R-1, 55–60 cm = silica-pyrophyllite alteration.

lated, whereas most other major and trace elements were lost from the rock.

3. Pyrophyllite alteration resulted in the loss of most of the major elements (except SiO_2 and Al_2O_3), and almost complete loss of Cs, Cu, Rb and Zn. For two of the samples this alteration style is also associated with the largest increases in the Cr and Pb (510 and 665% gains, respectively).

The chemical change calculations suggest that the uptake of most of the elements during the alteration of felsic rocks is most likely related to the hydrothermal formation of clay minerals (see next section).

The gain in Fe and Mg during chloritization corresponds with the formation of an Mg-rich chlorite. The presence of Mg-chlorite in several mid ocean ridge hydrothermal systems has been taken to indicate that the initial fluids were a mixture of hydrothermal fluids and seawater (e.g., Humphris et al., 1998; Lackschewitz et al., 2000a,b). The pattern of gains of elements during the chloritization of the felsic rocks is quite similar to those found at the midocean ridge TAG hydrothermal system, where a strong enrichment of Fe_2O_3, V, Co was observed (Humphris et al., 1998). However, chloritization in both systems resulted in depletion of CaO, Na_2O, Cu and Zn in the altered rock which correlates very well with results from basalt-seawater experiments at water/rock mass ratios greater than ~50 (Mottl, 1983).

The strong enrichment of Cr is a distinctive characteristic of all three alteration styles. A similar increase of Cr was also observed in altered compared to fresh basaltic andesites from the Desmos Caldera in the Manus Basin (Gena et al., 2001). Although traces of oxide phases such as chromite or spinel

might be thought to be the natural hosts for such elements in these samples, detailed petrographic studies of the samples (Pinto et al., 2004) show that such phases are not present in samples from the depth intervals studied here. The petrography shows that magnetite occurs in the matrix of most samples. The lack of a consistent Cr enrichment with Fe enrichment in Figure 7, the relatively low Cr contents of the magnetites analyzed by Pinto et al. (2004) and the very similar Nb and Ta contents of fresh and altered samples (two samples from the Leg 193 cores recovered from the relatively fresh cap rock (samples 1189A-1R-1, 0–4 cm and 1188A-2R-1, 1–3 cm) show Nb and Ta contents of 2.7, 2.2 and 0.18, 0.15 respectively) all suggest that magnetite is not the carrier responsible for the Cr enrichment in these samples. Natural micas have been described that contain major or significant amounts of Cr, V, Mn, Ba, Be and Zn (Newman and Brown, 1987). Cr is also a common trivalent cation in the octahedral sheets of some chlorites (Newman and Brown, 1987). In some chlorites the negative charge on the tetrahedral sheets, arising from substitution of Al^{3+} for Si^{4+}, is balanced simply by the inclusion of an equal number of trivalent cations, such as Cr^{3+}, in the octahedral sheets, the remaining sites being occupied by divalent cations. Substitutions are generally rare in the pyrophyllite structure (Newman and Brown, 1987). However, a few medium-sized cations, such as Cr, Ni, V and Cu, can be substituted in the octahedral sites of pyrophyllite (see also later).

The gain of Al_2O_3 and K_2O during the illitization corresponds to an increasing abundance of illite. As described above the high Ba content could be the result of an incorporation into secondary illites. However, the Ba enrichment in the illitized sample can be also attributed to small amounts of barite (below the level detectable by XRD) in the sample. The similar explanation can probably be applied to the marked Pb enrichment in two of the bleached samples—even miniscule amounts of sulfides (e.g., sphalerite, 1.5% Pb at Pacmanus, Binns et al., 1993) in the analyzed samples could produce the Pb peak on Figure 7.

Calculated losses of K_2O, Na_2O, Fe_2O_3, MnO and, in the case of illitization, Si from the dacites during hydrothermal alteration at PACMANUS also correlate very well with results from rhyolite-seawater experiments where solutions gain significant portions of K, Na, Si, Fe and Mn with increasing temperature (Hajash and Chandler, 1981). The strong loss of CaO and Na_2O during the illitization and pyrophyllite alteration is most likely due to the alteration of plagioclase and volcanic glass.

Leaching experiments at 120°C have shown a high U mobility during reaction of rhyolitic glass (Zielinski, 1979). A high fraction of the U, and probably Th, is probably dissolved from glassy and crystalline felsic rocks during the illitization at temperatures above 200°C and sorbed on and/or incorporated into secondary illites from the hydrothermal fluids. Strong U enrichments are also reported for the oxidatively altered rocks from the Southwest Indian Ridge (Bach et al., 2001) and the oceanic crust south of the Costa Rica Rift Zone (Bach et al., 2003).

5.3.2. Trace Element Compositions of Clay Concentrates

Figure 4 shows that the clay concentrates have generally higher rare-earth element (REE) contents than the fresh rocks from the Pual ridge, although the shape of the REE patterns are similar. An overview of the changes in trace element composition during alteration is presented in Figure 8, in which the trace element concentrations of the pyrophyllites, chlorites and illites are normalized to the altered bulk rock samples from which they were derived (Fig. 8A) or the calculated precursor (Fig. 8B). The comparisons such as those shown in Figure 8A could be subject to errors due to the presence of trace impurities of other minerals within the clay concentrates. However, the minerals quartz, plagioclase, K-feldspar and anhydrite, detected in trace amounts in some of the clay concentrates by XRD, have clearly defined compositions and do not have the ion exchange capabilities of clay minerals—the possible chemical effects of their presence as impurities can therefore be clearly predicted. In the case of the pyrophyllites, sample 1188A-9R-1, 5–9 cm shows XRD traces of anhydrite, sample 1188A-10R-1, 39–43 cm traces of quartz and 1188A-14R-1, 55–60 cm appears pure. Of these minerals, quartz will not contain significant quantities of the trace elements considered in Figure 8 and so the presence of trace quartz is not relevant to the trace element budgets. Anhydrite may contain Sr and Ba substituting for Ca. The pyrophyllite samples show identical or lower Ba and Sr concentrations normalized to their bulk altered rock (Fig. 8A) and so no chemical trace of contaminating anhydrite is evident in sample 1188A-9R-1.

The presence of alteration-resistant primary minerals such as apatite or rutile in the clay concentrates at concentrations below those detectable by XRD can also be excluded on geochemical grounds. Rutile (TiO_2, 60 wt% Ti) would be primarily detectable by its effect on the Ti content of the concentrates. Relative to the precursors shown in Table 8, we see that only the chlorite separates 1189A-13R-1 and 1189B-10R-1 in Table 4 show somewhat elevated Ti contents (ca. 0.6 wt% TiO_2 more than the average precursors). Such a TiO_2 increase could be caused by $< 1\%$ contamination of these two concentrates with rutile—the effects of such small amounts of contamination on the trace elements would only be relevant for Nb and Ta (with mineral/melt partition coefficients of 100–500, Foley et al., 2000). Table 5 shows the chlorite separates in question to have, if anything, lower Nb contents than the other concentrates. These low Nb concentrates also allow us to exclude significant zircon contamination in the concentrates—zircon shows distribution coefficients >200 for Nb (Thomas et al., 2002). Apatite has an appreciable affinity only for the middle REE (e.g., Green, 1994). The presence of small amounts of apatite in the concentrates should therefore generate a convex-upward REE pattern on Figure 8B—the patterns tend to be convex downward rather than upward, hence showing no evidence for apatite contamination.

We have only one chlorite/bulk altered sample and illite/bulk altered sample pair for comparison. The XRD analysis of sample 1188F-18Z-1, 13–17 cm shows no signs of traces of other minerals and so the illite must be classified as pure. The chlorite concentrate from sample 1188A-20R-1, 68–72 cm shows traces of illite and plagioclase contamination in the XRD spectrum. The effects of plagioclase contamination are predictable (Sr, Eu enrichment) but are not evident in the chlorite vs altered sample pattern (Fig. 8A) leading us to conclude that the plagioclase does not significantly affect the trace element signature of the clay concentrate. Figure 8A also shows that illite has lower enrichment factors relative to the altered bulk rock

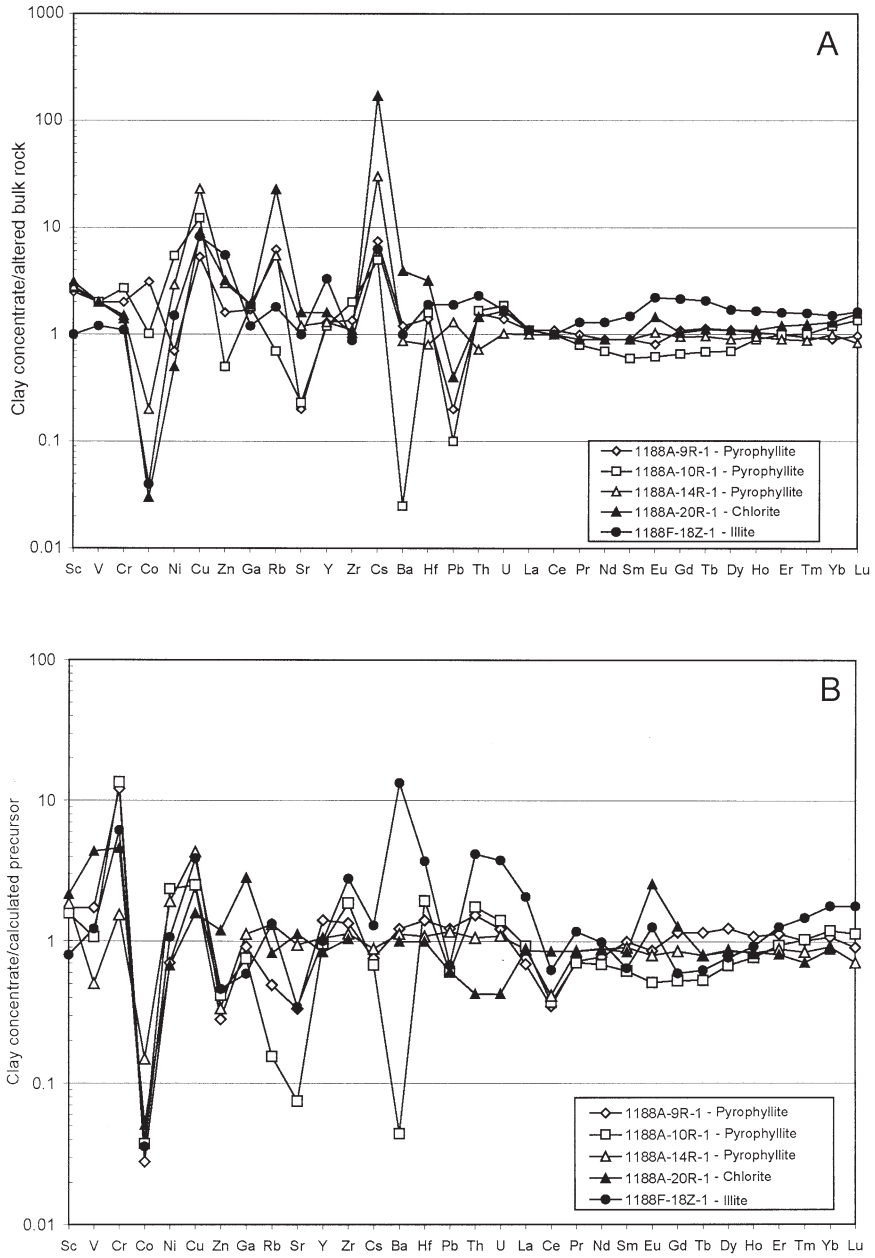

Fig. 8. Trace element distribution diagrams for near-monomineralic pyrophyllites, chlorites and illites normalized to the altered bulk rock samples from which they were derived (A) and the calculated precursor (B).

than chlorite, demonstrating that the marked enrichments in, for example, Rb, Cs and Hf cannot be due to illite impurities in the chlorite concentrate.

When we compare the chemical differences between pyrophyllite concentrates and altered bulk rock (Fig. 8A) with those between altered bulk rock and calculated precursor (Fig. 7) we see some interesting effects. Two of the three bleached whole-rock samples show over 500% enrichment in Pb in Figure 7. The clay concentrate data show clearly that this Pb is not predominantly present in the clays—they show strong negative anomalies in Figure 8A. Cs, Rb and Cu on the other hand are in all three pyrophyllite-rich samples the most strongly depleted elements in the bulk altered samples relative to the calculated precursors (Fig. 7). The pyrophyllite concentrates show clear positive anomalies for these three elements on Figure 8A, indicating that the Cs, Rb and Cu lost from igneous minerals were retained in the clays. This point can be further emphasized by comparing the clay concentrates directly with the calculated precursors (Fig. 8B). We see for example that Cs in the pyrophyllite concentrates, whilst strongly enriched relative to bulk altered rock, is approximately at the same concentration as in the calculated precursor. This suggests that during alteration the other minerals in the altered rock have lost most of their Cs, the clays have incorporated the igneous Cs. A similar situation is seen for Rb, although here even the clays may have lost some Rb. The Cu enrichment in the pyrophyllites

relative to the altered bulk rock is mirrored in the Cu enrichment relative to the precursor—it seems that the pyrophyllites are the main carrier of Cu in the bleached samples. A similar conclusion can be drawn for Cr. Co concentrations decrease generally during bleaching, Figure 8B shows that the pyrophyllites in particular are extremely depleted in Co.

There are some significant differences in the trace element behavior of the other clay minerals compared to pyrophyllite. Chlorite is clearly a major carrier for Hf in the altered rocks, more so than pyrophyllite (Fig. 8A). The enrichments in Th, U and Ba seen in the illite-rich rock relative to the precursors (Fig. 7) appear to be related to a general increase in the concentrations of these elements during alteration: relative to the altered bulk rock, the illite concentrate shows no marked enrichments in these elements (Fig. 8A). Only for Cs and Cu does illite show a significant enrichment relative to the bulk altered sample.

5.4. Composition of the Hydrothermal Fluids

Distinct mineralogical and geochemical differences in the alteration assemblages appear to have been caused by different types of precursors, temperatures and varying proportions of seawater and hydrothermal fluids.

5.4.1. Chlorite Formation

The replacement of volcanic rock by a nearly monomineralic chlorite assemblage is the result of magnesium metasomatism caused by reaction of seawater with hot hydrothermal fluid upwelling through the volcanic succession of Pual Ridge. The immobile Zr/TiO_2 of the bulk altered rock from which the single analyzed chlorite concentrate was prepared shows its precursor to have been dacite. Studies of midocean ridge hydrothermal systems, in which basalt is the predominant precursor, show that chlorite is the most commonly formed alteration product (e.g., Humphris et al., 1998). Chlorite is however also generated by the alteration of other precursors, although not in the same quantities. Based on mineral stability, the formation of authigenic chlorite and chlorite mixed-layer clays requires a fluid with a relatively high Mg^{2+}/H^+ ratio, that is, neutral to slightly acid pH assuming seawater Mg content. The hydrolytic alteration by slightly acid fluids will enhance dissolution of feldspar and pyroxene and lead to the removal of cations from the rocks.

5.4.2. Illite Formation

Hydrothermal experiments by Yates and Rosenberg (1998) indicate a prograde reaction toward end-member illite via stepwise formation of solubility-controlling mixed-layer phases with increasing K-contents. Although Yeh and Savin (1977) have suggested that I-S mixed layers will be formed between 220 and 270°C, Yates and Rosenberg (1998) have demonstrated the stability of end-member illite in the system K_2O-Al_2O_3-SiO_2-H_2O at 250°C. The formation of illite along with I-S requires a fluid with higher K^+/H^+ than the value (log $K^+/H^+ = 1.5$) calculated for vent fluids sampled at PACMANUS chimneys (Douville, 1999).

Several studies have indicated that illite-smectite mixed-layer is commonly formed by direct crystallization from fluids (Alt and Jiang, 1991; Suharno et al., 1999; Ylagan et al. 2000). However, other studies conclude that illitization is a multiple reaction event where smectite reacts to form illite through mixed-layer illite-smectite (Inoue et al., 1987). In this multistep model, temperature of alteration and K^+ availability provide the major controls. Other factors that may play a role include water-rock ratio and permeability (Ylagan et al., 2000).

5.4.3. Pyrophyllite Formation

Pyrophyllite formation has been previously described from fossil ore deposits, e.g., the Kuroko deposits of Japan (Marumo, 1989), geothermal systems such as Otake area in Japan (Hayashi, 1973) and seafloor hydrothermal sites such as Desmos Caldera (Gena et al., 2001). Pyrophyllite is most frequently found in very aluminous rocks and in rocks relatively enriched in Al by base-leaching during hydrothermal alteration (Evans and Guggenheim, 1988). Hayashi (1973) noted that pyrophyllite forms at temperatures above 230°C in the Otake geothermal system whereas in the Desmos caldera the stability of pyrophyllite is restricted to acidic solutions at temperatures between 260–340°C (Gena et al., 2001). Experimental work in the system Al_2O_3-SiO_2-H_2O (e.g., Hemley et al., 1980) shows that both high SiO_2-activity and high temperature are necessary to form pyrophyllite. Phase stability calculations carried out with the GWB software package (www.rockware.com) by Yeats et al. (2001) show pyrophyllite and quartz to be the only stable mineral phases in contact with fluids sampled at PACMANUS chimneys (Douville, 1999). We conclude that the pyrophyllite found in the Leg 193 cores precipitated from such fluids most probably as they cooled conductively when approaching the seafloor.

5.5. Source of Fluids for Alteration

In view of the large differences in concentration and isotopic composition of Sr between the pristine rock from the Pual Ridge (Sr = ca. 250 ppm, $^{87}Sr/^{86}Sr = 0.70358$; unpublished data of R. Binns), seawater (Sr = 8 ppm, $^{87}Sr/^{86}Sr = 0.70918$) and the end-member black-smoker fluids (Sr = 9 ppm, $^{87}Sr/^{86}Sr = 0.705$, determined by extrapolation to Mg = 0 from data of Douville, 1999), measurements of Sr isotope ratios in the secondary clays are ideal for determining what fluids were responsible for the alteration. Note that impurities in the mineral concentrates, if present, would have the following effects on the measured Sr isotope ratios of the concentrates: Primary minerals: Quartz—no effect, feldspar—move ratio towards mantle value; secondary minerals: anhydrite—move value towards seawater. The evidence from XRD and trace element considerations presented above (see section 5.3.2) suggests that the geochemical effects of any impurities will be negligible, however. Previous work on other hydrothermal fields (e.g., TAG; Teagle et al., 1998) has shown a steady decrease in $^{87}Sr/^{86}Sr$ ratio with depth from near seawater ratios close to the seafloor to black-smoker-like values at depth. $^{87}Sr/^{86}Sr$ measurements on vein anhydrites from Leg 193 drill cores studies here have shown large differences in the fluid sources for Snowcap and Roman Ruins (Roberts et al., 2003). Figure 5 shows the situation at Snowcap from the clay mineral viewpoint. In the upper parts of the system (<120 mbsf), the

$^{87}Sr/^{86}Sr$ ratio of the clays cluster around that of the hydrothermal fluid. These samples are also the only ones in which pyrophyllite occurs, suggesting on mineral stability grounds that the fluid is dominated by the hot, acidic, Si-rich hydrothermal component. The first chlorite sample from Snowcap (175 mbsf) has a Sr isotopic ratio clearly *below* that of the end-member black-smoker fluid, suggesting a strong contribution to the Sr budget from leaching of the magmatic rocks at this depth. Indeed, the relatively low Sr isotope values of all the clays between 100–200 mbsf show that the contribution of seawater Sr to the altering fluid at these depths was minor.

The abundance of anhydrite decreases markedly between approximately 160–200 m (Binns et al., 2002). The one clay sample we have from ca. 175 mbsf shows the lowest Sr isotope ratio measured, suggesting precipitation from fluid with very low seawater contents. This may account for the paucity of anhydrite in this section—low proportions of seawater in the fluid lead to low sulfate concentrations and so only limited anhydrite precipitation.

The isotope ratios in both anhydrites and clays increase again with depth below 220 mbsf and at all greater depths stay above the end-member black-smoker values, probably indicating deep lateral recharge with more seawater-rich (up to 30%) fluids at this site. In contrast to Snowcap, the strontium isotopic ratios of clay minerals from Roman Ruins are all below those of the black-smoker fluid and are much lower than the isotopic data reported for the anhydrites.

We have attempted to investigate the fluids involved in the mixing using information from the Sr concentrations (Fig. 9). On this figure, the use of 1/Sr results in mixing lines being straight. Most of the clays measured lie to the left of linear mixing lines between parent rock and either hydrothermal fluid or seawater. We consider this to indicate that the secondary clays have derived all of their Sr from the fluid with no direct incorporation of rock Sr into the secondary clays. During crystallization of the clay minerals, the partitioning of Sr between fluid and clay has then played a major role. We have modeled this using a simple model of crystallization from a seawater-rock mix using a K_d (water/clay) of 0.1. This partition coefficient was used as it represents the average concentration ratio Sr end-member fluid/Sr clay. The influence of these partition coefficients also explains the consistent deficit in Sr in the alteration products relative to the calculated precursors seen in Figures 7 and 8.

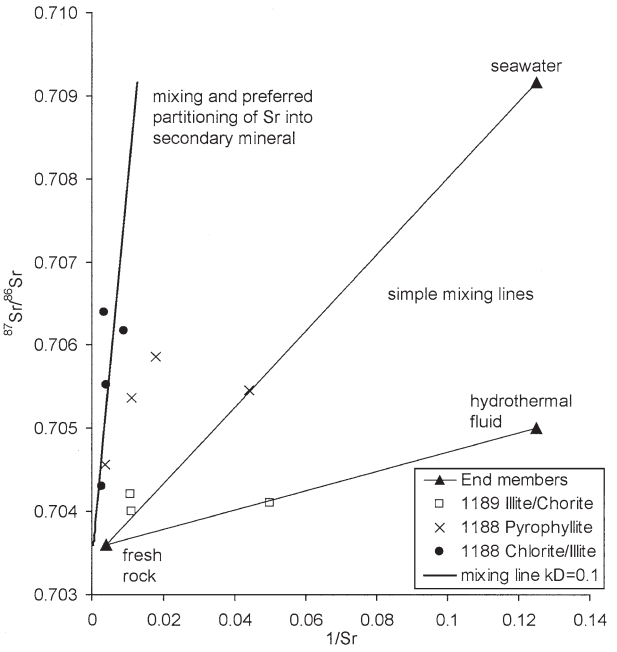

Fig. 9. Sr isotope compositions versus 1/Sr content for secondary clays and possible end members contributing to fluid composition. Mixing lines between rock and either seawater or local black-smoker fluid are shown. Most clay data fall to the left of these lines, indicating that the clays have higher Sr concentrations than a direct mixture between the two end members, suggesting that the clays have a distribution coefficient for Sr (K_d) < 1. A modeled mixing and partitioning curve using $K_d = 0.1$ is shown.

5.6. The PACMANUS Hydrothermal System

The observations and conclusions derived from the mineralogy, geothermometry and geochemistry are summarized schematically in Figure 10. Both sites are characterized by high temperatures in the upper part of the sequence directly below the capping rock (unaltered lava). In the case of Roman Ruins, the exceptionally high temperatures found in the upper parts of the sequence were measured in quartz veins and as such are not directly related to the clay mineral parageneses from which the other temperature information was derived.

The high temperature upper zone is underlain at Snowcap by a region with distinctly lower temperatures, and the temperatures then increase steadily downwards as illustrated in Figure 10. Such a temperature profile is strong evidence for advective heat transfer by fluids. A similar conclusion has also been reached by Vanko et al. (2004) from studies of fluid inclusions. The lower temperature region in zone 2 at Snowcap is associated with low Sr isotope ratios in the authigenic clays and an absence of anhydrite, both suggesting that seawater penetrates only weakly, if at all, into this region. We associate the lower temperatures therefore with a return flow of cooled hydrothermal solution from above. Roman Ruins also shows lower temperatures (ca. 220°C) beneath the high-temperature upper regions. However, we see no change to increasing temperatures with depth at the base of the core, presumably as the penetration was not deep enough to encounter the true geothermal gradient.

The mineralogical and chemical information presented here gives no information about the relative timing of these different alteration processes. Shipboard mineralogical information (Shipboard Scientific Party, 2002; Binns et al., 2002) allow a crude chronology to be deciphered, however. According to this work, early alteration produces a pervasive green coloration comprising silica polymorphs, illite and chlorite with some associated pyrite. This is overprinted by bleaching, involving the development of clays, pyrophyllite and variable amounts of pyrite and anhydrite in haloes around veins. A late-stage silicification may follow the bleaching. In all areas the rocks are cut by pervasive late-stage anhydrite veins which may also contain traces of pyrite (e.g., Vanko et al., in press).

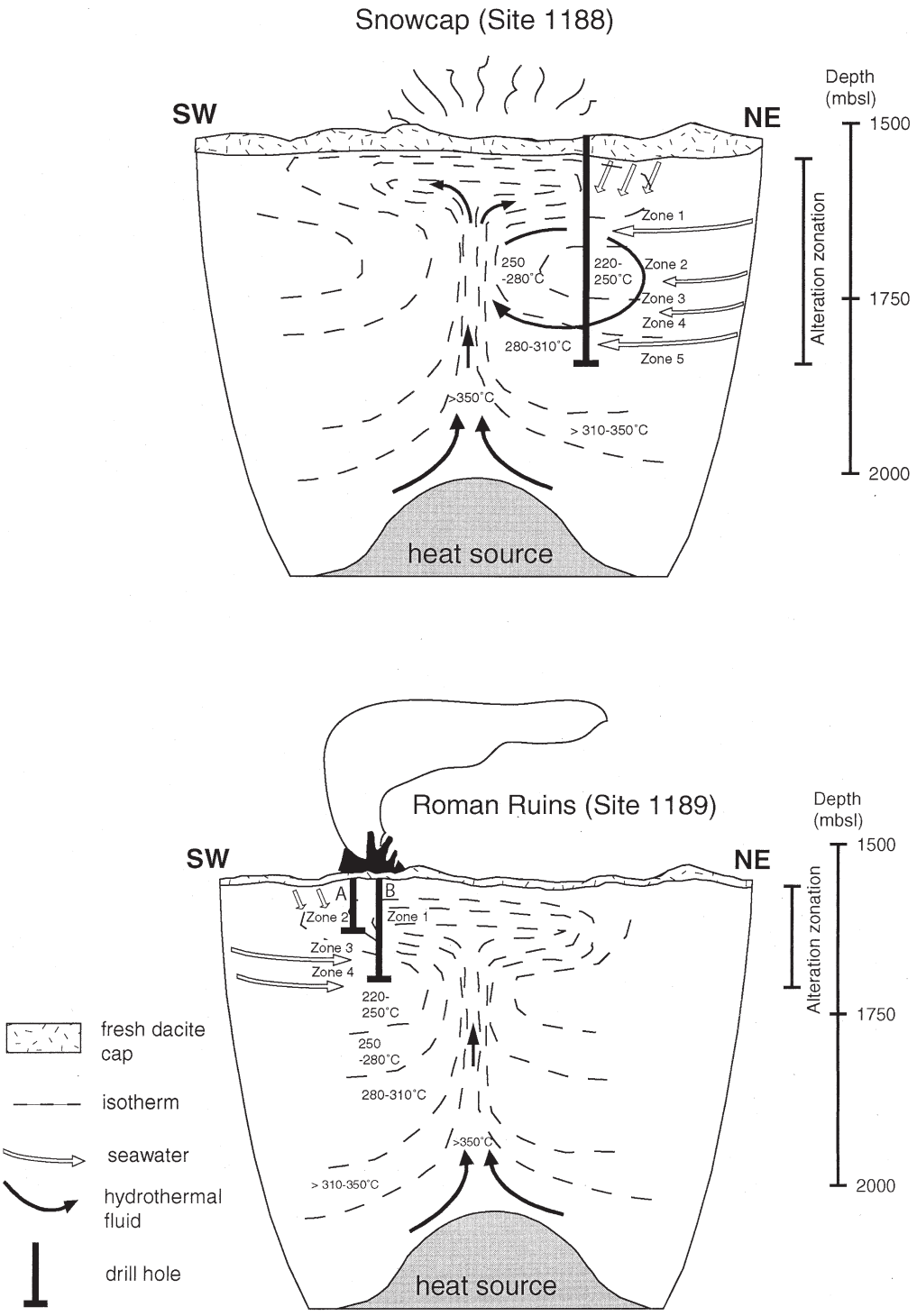

Fig. 10. Schematic diagram depicting the hydrothermal alteration changes at Snowcap (Site 1188) and Roman Ruins (Site 1189). General fluid flow pathways and isotherms are inferred from mineralogy and temperature estimates from oxygen isotope data.

6. CONCLUSIONS

Studies of the mineralogy and geochemistry of altered rocks recovered from ODP Leg 193 holes lead to the following conclusions:

- The felsic-hosted alteration systems at PACMANUS are characterized by a large range of alteration mineral assemblages, much larger than is found at basalt-hosted midocean ridge systems. Particularly striking is the presence of a wide range of mixed two- and three-layer sheet silicates, varieties

that have not previously been described from other midocean ridge hydrothermal systems.

- The temperature-depth profiles derived from the mineral thermometry show clear maxima close to the surface, reflecting the dominance of convective rather than conductive heat transfer and the importance of the capping seal of fresh eruptives in the PACMANUS hydrothermal systems.
- The chloritization, illitization and pyrophyllite-bearing alteration styles show differing chemical changes in the altered samples relative to a calculated pristine precursor lava. The element Cr appears to have a general enrichment in the altered bulk samples. A particularly marked enrichment in Cu and Cr is evident in the pyrophyllite concentrates. Rb and Cs are notably enriched in a chlorite concentrate. Cs and Cu are significantly enriched in illite concentrates.
- Mineral stability considerations allow constraints to be placed on fluid chemistry. The change from chloritization/illitization to bleaching must be accompanied, for example, by a reduction in pH from ≥ 5 by chloritization to < 3 during bleaching. Pyrophyllite formation is also only possible under conditions of high SiO_2-activity.
- The fluid responsible for the hydrothermal clay alteration was most probably a mixture of upwelling, high temperature (>220°C), black smoker-type fluid with minor ($<30\%$) proportions of seawater.

Acknowledgments—The authors gratefully acknowledge Dietrich Ackermand for electron microprobe analyses; Heike Anders and Andreas Klügel for technical assistance with ICP-MS analyses; Inge Dold (Kiel University) for sample preparation and Manfred Schmitt (Sehnde-Ilten) and Monika Segl (Bremen University) for oxygen isotope analyses, Ana Kolevica for sample preparation for strontium isotope analyses; and Anna Ksienzyk and Holger Strauss for help with sample preparation. We thank the Master and crew of JOIDES Resolution, the Ocean Drilling Program personnel and the other members of the shipboard scientific party for constructive collaboration. Wolfgang Bach and Chris Yeats provided quartz separates for oxygen isotope analyses and precursor concentrations for altered whole rock samples, respectively. Discussions with Wolfgang Bach and Holger Paulick were most beneficial. Constructive reviews by Ray Binns, Martine Buatier, Steve Scott and an anonymous reviewer, and helpful comments by the associate editor Jeff Alt lead to substantial improvements in the manuscript. Samples were provided by the Ocean Drilling Program (ODP). ODP is sponsored by the U.S. National Science Foundation (NSF) and participating countries under management of Joint Oceanographic Institutions (JOI), Inc. This research has been supported by the Deutsche Forschungsgemeinschaft (DFG), Bonn, via grant STO 110/36-1 and DE 572/12-1.

Associate editor: J. Alt

REFERENCES

Alt J. C., Teagle D. A. H., Brewer T., Shanks W. C.III, and Halliday A. N. (1998) Alteration and mineralization of an ocean forearc and the ophiolite-ocean crust analogy. *J. Geophys. Res*. **103,** 12365–12380.

Alt J. C. and Jiang W.-T. (1991) Hydrothermally precipitated mixed-layer illite-smectite in recent massive sulfide deposits from the sea floor. *Geology* **19,** 570–573.

Alt J. C. and Bach W. (2003) Alteration of oceanic crust: Subsurface rock-water interactions. In *Energy and Mass Transfer in Marine Hydrothermal Systems,* Dahlem Workshop Report 89 (eds. P. E. Halbach, V. Tunnicliffe, and J. R. Hein), pp. 7–27. Dahlem University Press.

Auzende J.-M., Urabe T., and Scientific Party of ManusFlux Cruise. (1996) Submersible observation of tectonic, magmatic and hydrothermal activity in the Manus Basin (Papua New Guinea). *Eos* **77,** W115.

Bach W., Alt J. C., Nio Y., Humphris S. E., Erzinger J., and Dick H. J. B. (2001) The geochemical consequences of late-stage low-grade alteration of lower ocean crust at the SW Indian Ridge: Results from ODP Hole 735B (Leg 176). *Geochim. Cosmochim. Acta* **65** (*19*), 3267–3287.

Bach W., Peucker-Ehrenbrink B., Hart S. R., and Blusztajn J. S. (2003) Geochemistry of hydrothermally altered oceanic crust: DSDP/ODP Hole 504B—Implications for seawater-crust exchange budgets and Sr- and Pb-isotopic evolution of the mantle. *Geochem. Geophys. Geosys.* **4** (*3*), 29.

Barrie C. T., Hannington M. D. (1999) Volcanic-associated massive sulfide deposits: Processes and examples in modern and ancient settings. *Rev. Econ. Geol*. **8,** 373.p.

Binns R. A. and Scott S. D. (1993) Actively forming polymetallic sulfide deposits associated with felsic volcanic rocks in the eastern Manus back-arc basin, Papua New Guinea. *Econ. Geol.* **88,** 2226–2236.

Binns R. A., Barriga F. J. A. S., Miller D. J., et al. (2002) *Proc. ODP, Init. Results*, Vol. 193. Ocean Drilling Program.

Borthwick J. and Harmon R. S. (1982) A note regarding ClF_3 as an alternative to BrF_3 for oxygen isotope analysis. *Geochem. Cosmochim. Acta* **46,** 1665–1668.

Brindley G. W. and Brown G. (1980) *Crystal Structures of Clay Minerals and Their X-ray Identification*. London Mineralogical Society. Monograph No. 5.

Buatier M., Honnorez J., and Ehret G. (1989) Fe-smectite-glauconite transition in hydrothermal green clays from the Galapagos spreading center. *Clays Clay Minerals* **37** (*6*), 532–541.

Buatier M. D., Früh-Green G. L., and Karpoff A. M. (1995) Mechanism of Mg-phyllosilicate formation in a hydrothermal system at a sedimented ridge (Middle Valley, Juan de Fuca). *Contrib. Mineral. Petrol.* **122,** 134–151.

Clayton R. N. and Mayeda T. K. (1963) The use of bromine pentafluoride in the extraction of oxygen from oxides and silicates for isotopic analysis. *Geochem. Cosmochim. Acta* **27,** 43–52.

Cole D. R. and Ripley E. M. (1998) Oxygen isotope fractionation between chlorite and water from 170 to 350°C: A preliminary assessment based on partial exchange and fluid/rock experiments. *Geochim. Cosmochim. Acta* **63** (*3/4*), 449–457.

Cole D. R., Riciputi L. R., and Horita J. (1998) Stable isotope exchange equilibria and kinetics in mineral-fluid systems. In *Proceedings of the 9th International Symposium on Water-Rock Interaction* (eds. G. B. Arehart and J. R. Hulston), pp. 827–830. Balkema.

Corbett G. J. and Leach T. M. (1998) Southwest Pacific rim gold-copper system: Structure, alteration, and mineralization. Spec. Publ. 6. Soc. Econ. Geol.

Douville E. (1999) Les fluides hydrothermaux océaniques: Comportement géochimique des éléments traces et des terres rares. Processus associés et modélisation thermodynamique. Ph.D. thesis. University of Western Brittany, Brest, France.

Evans B. W. and Guggenheim S. (1988) Talc, pyrophyllite, and related minerals. In *Hydrous Phyllosilicates (Exclusive Micas)* (ed. S. W. Bailey). *Rev. Mineral*. **19,** 225–294. The Mineralogical Society of America, Washington D.C.

Foley S. F., Barth M. G., and Jenner G. A. (2000) Rutile/melt partition coefficients for trace elements and an assessment of the influence of rutile on the trace element characteristics of subduction zone magmas. *Geochim. Cosmochim. Acta* **64** (*5*), 933–938.

Foster M. D. (1962) Interpretation of the composition and a classification of the chlorites. Prof. Pap. 414-A. Geol. Surv.

Gamo T., Okamura K., Charlou J.-L., Urabe T., Auzende J.-M., Ishibashi J., Shitashima K., and Chiba H. (1997) Acidic and sulfate-rich hydrothermal fluids from the Manus back-arc basin, Papua New Guinea. *Geology* **25,** 139–142.

Garbe-Schönberg D. (1993) Simultaneous determination of 37 trace elements in 28 international rock standards by ICP/MS. *Geostandards Newslett*. **17,** 81–97.

Gena K., Mizuta T., Ishiyama D., and Urabe T. (2001) Acid-sulphate type alteration and mineralization in the Desmos Caldera, Manus Back-arc Basin, Papua New Guinea. *Res. Geol.* **51** (*1*), 31–44.

Grant J. A. (1986) The isocon diagram—A simple solution to Gresen's equation for metasomatic alteration. *Econ. Geol*. **81,** 1976–1982.

Green T. H. (1994) Experimental studies of trace-element partitioning applicaple to igneous petrogenesis—Sedona 16 years later. *Chem. Geol*. **117,** 1–36.

Gresens R. L. (1967) Composition-volume relationships of metasomatism. *Chem. Geol*. **2,** 47–65.

Hannington M. D., Jonasson I. R., Herzig P. M., and Petersen S. (1995) Physical and chemical processes of seafloor mineralization at mid-ocean ridges. In *Seafloor Hydrothermal Systems: Physical, Chemical, Biological, and Geological Interactions*, Geophysical Monograph 91 (eds. S. E. Humphris, R. A. Zierenberg, L. S. Mullineaux, and R. E. Thomson), pp. 115–157. American Geophysical Union.

Hajash A. and Chandler G. W. (1981) An experimental investigation of high-temperature interactions between seawater and rhyolite, andesite, basalt, and peridotite. *Contrib. Min. Petrol*. **78,** 240–254.

Hajashi M. (1973) Hydrothermal alteration in the Otake geothermal area, Kyushu. *J. Jpn. Geotherm. Energy Assoc*. **10,** 9–46.

Hemley J. J., Montoya J. W., Marinenko J. W., and Luce R. W. (1980) Equilibria in the system Al_2O_3-SiO_2-H_2O and some general implications for alteration/mineralization processes. *Econ. Geol*. **75,** 210–228.

Herzig P. M., Hannington M. D., Fouquet Y., von Stackelberg U., and Petersen S. (1993) Gold-rich polymetallic sulfides from the Lau back-arc and implications for the geochemistry of gold in seafloor systems of the south-west Pacific. *Econ. Geol*. **88,** 2182–2209.

Herzig P. M. and Hannington M. D. (2000) Polymetallic massive sulfides and gold mineralization at mid-ocean ridges and in subduction-related environments. In *Handbook of Marine Mineral Deposits* (ed. D. S. Cronan), pp. 347–368. CRC Press.

Hey M. H. (1954) A new review of the chlorites. *Min. Mag*. **30,** 277–292.

Honnorez J., Karpoff A. M., and Trauth Badaut D. (1983) Sedimentology, mineralogy and geochemistry of green clay samples from the Galapagos hydrothermal mounds, holes 506, 506C, and 507D Deep Sea Drilling Project Leg 70. In *Init. Repts. Deep Sea Drilling Project, Vol. 70* (eds. J. Honnorez et al.), pp. 221–224. U.S. Government Printing Office.

Humphris S. E., Alt J. C., Teagle D. A. H., and Honnorez J. J. (1998) Geochemical changes during hydrothermal alteration of basement in the stockwork beneath the active tag hydrothermal mound. In *Proc. ODP Sci. Results*, Vol. 158 (eds. P. M. Herzig, S. E. Humphris, D. J. Miller, and R. A. Zierenberg), pp. 255–276. Ocean Drilling Program.

Inoue A., Kokyama N., Kilagawa R., and Watanabe T. (1987) Chemical and morphological evidence for the conversion of smectite to illite. *Clays Clay Minerals* **35,** 111–120.

Kear D. (1989) Geology of the Wharekirauponga epithermal gold deposit, Coromandel region. In *Mineral deposits of New Zealand: A collection of papers summarising the results of mineral exploration in New Zealand 1974–87,* Vol. 13, pp. 93–97. Australasian Institute of Mining and Metallurgy.

Knauth L. P. and Epstein S. (1976) Hydrogen and oxygen isotope ratios in nodular and bedded cherts. *Geochim. Cosmochim. Acta* **40,** 1095–1108.

Lackschewitz K. S., Singer A., Botz R., Garbe-Schönberg D., Stoffers P., and K. Horz (2000a) Formation and transformation of clay minerals in the sedimentary sequence of Middle Valley, Juan de Fuca Ridge, ODP Leg 139 and 169. *Econ. Geol*. **95,** 361–390.

Lackschewitz K. S., Singer A., Botz R., Garbe-Schönberg D., and Stoffers P. (2000b) Mineralogical and geochemical characteristics of clay minerals in the region of a major hydrothermal site in the Escanaba Trough, Gorda Ridge, northeast Pacific Ocean, Leg 169. In *Proc. ODP Sci. Results, Vol. 169* (eds. R. A. Zierenberg, Y. Fouquet, D. J. Miller, and W. R. Normark), pp. 1–24. Ocean Drilling Program.

Marumo K. (1989) Genesis of kaolin minerals and pyrophyllite in Kuroko deposits of Japan: Implications for the origins of the hydrothermal fluids from mineralogical and stable isotope data. *Geochim. Cosmochim. Acta* **53,** 2915–2924.

Matsuhisa Y. (1974) $^{18}O/^{16}O$ ratios for NBS-28 and some silicate reference samples. *Geochem. J.* **8,** 103–107.

Mehra O. P. and Jackson M. L. (1960) Iron oxide removal from soils and clays by dithionite-citrate system buffered with sodium bicarbonate. *Clays Clay Minerals.* **7,** 317–327.

Moore D. M. and Reynolds R. C. (1989) *X-ray Diffraction and the Identification and Analysis of Clay Minerals*. Oxford University Press.

Moss R., Scott S. D., and Binns R. (2001) Gold content of eastern Manus basin volcanic rocks: Implications for enrichment in associated hydrothermal precipitates. *Econ. Geol*. **96,** 91–107.

Mottl M. J. (1983) Metabasalts, axial hot springs, and the structure of hydrothermal systems at mid-ocean ridges. *Geol. Soc. Am. Bull*. **94,** 161–180.

Newman A. C. D. and Brown G. (1987) The chemical constitution of clays. In *Chemistry of Clay and Clay Minerals* (ed. A. C. D. Newman), pp. 1–480. Monograph 6. Mineralogical Society.

Paulick H., Vanko D. A., and Yeats C. J. (2004) Drill core-based facies reconstruction of a deep-marine felsic volcano hosting an active hydrothermal system (Pual Ridge, Papua New Guinea, ODP Leg 193). *J. Volcanol. Geotherm. Res*. **130** (*1–2*), 31–50.

Pinto A. M. M., Barriga F. J. A. S., and Scott S. D. (2004) Data report. Sulfide and oxide mineral chemistry of an active backarc hydrothermal system: PACMANUS, ODP Holes 1188A, 1188F, 1189A, and 1189B. In *Proc. ODP Sci. Results*, Vol. 193 (eds. F. J. A. S. Barriga, R. A. Binns, D. J. Miller, and P. M. Herzig), pp. 1–31. Ocean Drilling Program.

Porter S., Vanko D. A., and Ghazi A. M. (2000) Major and trace element compositions of secondary clays in basalts altered at low temperature, eastern flank of the Juan de Fuca Ridge. In *Proc. ODP Sci. Results*, Vol. 168 (eds. A. Fisher, E. E. Davies, and C. Escutia), pp. 149–157. Ocean Drilling Program.

Reynolds R. C. Jr. (1988) Mixed layer chlorite minerals. In *Hydrous Phyllosilicates (Exclusive Micas)* (ed. S. W. Bailey). *Rev. Mineral*. **19,** 601–629. The Mineralogical Society of America, Washington, D.C.

Roberts S., Bach W., Binns R. A., Vanko D. A., Yeats C. J., Teagle D. A. H., Blacklock K., Blusztajn J. S., Boyce A. J., Cooper M. J., Holland N., and McDonald B. (2003) Contrating evolution of hydrothermal fluids in the PACMANUS system, Manus Basin: The Sr and S isotope evidence. *Geology* **31** (*9*), 805–808.

Savin S. M. and Lee M. (1988) Isotopic study of phyllosilicates. In *Hydrous Phyllosilicates (Exclusive Micas)* (ed. S. W. Bailey). *Rev. Mineral*. **19,** 189–223.

Schöps D. and Herzig P. (1994) Hydrothermally altered felsic rocks of the Tonga Forearc. In *Proc. ODP Sci. Results, Vol. 135* (eds. J. W. Hawkins, L. M. Parson, J. F. Allan, and E. M. Maddox), pp. 653–663. Ocean Drilling Program.

Schiffman P. and Fridleifsson G. O. (1991) The smectite-chlorite transition in drillhole NJ-15, Nesjavellir geothermal field, Iceland: XRD, BSE and electron microprobe investigations. *J. Metamorph. Geol*. **9,** 679–696.

Shanks W. C. III, Böhlke J. K., and Seal R. R. II (1995) Stable isotopes in mid-ocean ridge hydrothermal systems: Interaction between fluids, minerals, and organisms. In *Seafloor Hydrothermal systems: Physical, Chemical, Biological, and Geological Interactions,* Geophysical Monograph 91 (eds. S. E. Humphris, R. A. Zierenberg, L. S. Mullineaux, and R. E. Thomson), pp. 194–221. American Geophysical Union.

Singer A. and Stoffers P. (1987) Mineralogy of a hydrothermal sequence in a core from the Atlantis II Deep, Red Sea. *Clay Min*. **22,** 251–267.

Sheppard S. M. F. and Gilg H. A. (1996) Stable isotope geochemistry of clay minerals. *Clay Min*. **31,** 1–24.

Shipboard Scientific Party (2002) Leg 193 summary. In *Proceedings of the Ocean Drilling Program, Initial Reports, 193* (eds. R. A. Binns, F. J. A. S. Barriga, D. J. Miller, et al.), pp. 1–84. Ocean Drilling Program.

Shitashima K., Gamo T., Okamura K., and Ishibashi J. (1997) Trace elements at the Manus Basin, Papua New Guinea. *JAMSTEC J. Deep Sea Res*. **13,** 249–255.

Suharno P., Browne P. R. L., Soengkono S., and Sudarman S. (1999) Hydrothermal clay minerals in the Ulebelu Geothermal field, Lampung, Indonesia. *New Zeal. Geotherm. Workshop* **21,** 95–100.

Sun S. S. and McDonough W. F. (1989) *Chemical and Isotopic Systematics of Oceanic Basalts: Implications for Mantle Composition and Processes*. Special Publication 42. Geological Society of London.

Teagle D. A. H., Alt J. C., Humphris S. E., and Halliday A. N. (1998) Dissecting an active hydrothermal deposit: The strontium and oxygen isotopic anatomy of the TAG hydrothermal mound—Whole rock and silicate minerals. In *Proc. ODP Sci. Results, Vol. 158* (eds. P. M. Herzig, S. E. Humphris, D. J. Miller and R. A. Zierenberg), pp. 297–309. Ocean Drilling Program.

Thomas J. B., Bodnar R. J., Shimizu N., and Sinha A. K. (2002) Determination of zircon/melt trace element partition coefficients from SIMS analysis of melt inclusions in zircon. *Geochim. Cosmochim. Acta* **66** (*16*), 2887–2901.

Vanko D. A., Bach W., Roberts S., Yeats C. J., and Scott S. D. (2004) Fluid inclusion evidence for subsurface phase separation and variable fluid mixing regimes beneath the deep-sea PACMANUS hydrothermal field, Manus Basin back-arc rift, Papua New Guinea. *J. Geophys. Res.* 109, B03201, doi: 10.1029/2003 JB002579.

Vitali F., Blanc G., Larqué P., Duplay J., and Morvan G. (1999) Thermal diagenesis of clay minerals within volcanogenic material from the Tonga convergent margin. *Mar. Geol*. **157,** 105–125.

Wenner D. B. and Taylor H. P. (1971) Temperatures of serpentinization of ultramafic rocks based on O^{18}/O^{16} fractionation between coexisting serpentine and magnetite. *Contrib. Mineral. Petrol.* **32,** 165–185.

Ylagan R. F., Altaner S. P., and Pozzuoli A. (2000) Reaction mechanism of smectize illitization associated with hydrothermal alteration from Ponza Island, Italy. *Clays Clay Minerals* **48** (*6*), 610–631.

Yates D. M. and Rosenberg P. E. (1998) Characterization of neoformed illite from hydrothermal experiments at 250°C and $P_{v,soln}$: An HRTEM/ATEM study. *Am. Mineral*. **83,** 1199–1208.

Yeats C. J., Bach W., Vanko D. A., Roberts S., Lackschewitz K. S., Paulick H., and ODP Leg 193 Shipboard Party (2001) Fluid-dacite interaction in the PACMANUS subseafloor hydrothermal system preliminary results from secondary mineral chemistry and geochemical modeling (abstract no. S011A-0346). *Eos* **82** (*47*).

Yeh H. W. and Savin S. M. (1977) Mechanism of burial metamorphism of argillaceous sediments: 3. O-isotope evidence. *Geol. Soc. Am. Bull*. **88,** 1321–1330.

Zielinski R. A. (1979) Uranium mobility during interaction of rhyolitic obsidian, perlite and felsite with alkaline carbonate solution: T = 120°C, P = 210Kg/cm^2. *Chem. Geol*. **27,** 47–63.

Zierenberg R. A. and Shanks W. C. III. (1994) Sediment alteration associated with massive sulfide formation in Escanaba trough, Gorda Ridge: The importance of seawater mixing and magnesium metasomatism. In *Geologic, Hydrothermal, and Biologic Studies at Escanaba Trough, Gorda Ridge, Offshore Northern California,* Bulletin, Vol. 2022 (eds. J. L. Morton, R. A. Zierenberg, and C. A. Reiss), pp. 257–278. U.S. Geological Survey.